The timing of blueschist-facies metamorphism in the Makrotantalon Unit on Andros Island, Greece: Cretaceous and Eocene high-pressure/low-temperature events?

Michael Bröcker[1] (ORCID), Erik E. Scherer[1], Paris Xypolias[2] and Melina Höhn[1]

[1]Institut für Mineralogie, Westfälische Wilhelms-Universität Münster, Corrensstr. 24, 48149 Münster, Germany and [2]Department of Geology, University of Patras, 26500 Patras, Greece

Abstract

This study corroborates interpretations suggesting that the Makrotantalon Unit on Andros represents a tectonic slice with Pelagonian affinity in the nappe stack of the Cycladic Blueschist Unit. Previously reported Cretaceous ^{40}Ar–^{39}Ar dates of a garnet-glaucophane schist from the Makrotantalon Unit could not be reproduced by Rb–Sr geochronology, but this is not an indication of contamination with excess Ar. Instead, the newly dated samples record disturbance of the Rb–Sr isotope system by partial recrystallization. Subsets of these phengite populations, representing the smaller grain-size fractions, yielded low-precision dates ranging from *c.* 21 to *c.* 15 Ma that document deformation-related resetting and recrystallization of a presumably Cretaceous white mica population. Although these Miocene dates cannot be linked with blueschist-facies metamorphism, they provide time constraints on the formation of shear zones that overprinted the original thrust contact during exhumation. The geological relevance of a Cretaceous high-pressure event is confirmed by a Rb–Sr date of *c.* 121 Ma for an epidote-glaucophane schist collected further away from the tectonic contact. The occurrence of a second blueschist-facies event in the Eocene is verified by Rb–Sr dates of two epidote-glaucophane schists (*c.* 40 Ma and *c.* 44 Ma) that can unambiguously be assigned to the Makrotantalon Unit.

CAMBRIDGE
UNIVERSITY PRESS

1. Introduction

The overall geological, magmatic and tectonometamorphic framework of the Attic-Cycladic crystalline belt (Fig. 1a) is well documented, but in detail there are still significant gaps in knowledge, particularly regarding geochronological aspects. One of these yet unresolved issues is the identification of tectonic slices within the Attic-Cycladic crystalline belt that have been affected by more than one high-pressure/low-temperature (HP/LT) metamorphic event (Gerogiannis *et al.* 2019). To address this point, we have studied blueschist-facies rocks from NW Andros (Figs 1, 2) where the metamorphic succession comprises two tectonic subunits, the Makrotantalon Unit and the Lower Unit (Papanikolaou, 1978*a,b*). On the basis of mineralogical and geochronological evidence, the Lower Unit of Andros can be correlated with the Cycladic blueschist sequences (= Cycladic Blueschist Unit), which underwent eclogite- to epidote-blueschist-facies metamorphism and subsequent overprinting at lower *P–T* conditions between *c.* 55 Ma and *c.* 12 Ma (e.g. Okrusch & Bröcker 1990; Wijbrans *et al.* 1990; Bröcker *et al.* 1993, 2013; Tomaschek *et al.* 2003; Lagos *et al.* 2007; Ring *et al.* 2010; Cliff *et al.* 2017; Peillod *et al.* 2017; Laurent *et al.* 2017, 2018; Lamont *et al.* 2020*b*; Glodny & Ring, 2022).

The status of the Makrotantalon Unit within the structural framework of the Attic-Cycladic crystalline belt is controversial, with some studies suggesting a relationship to the Cycladic HP/LT sequences (e.g. Papanikolaou, 1978*b*, 1987; Shaked *et al.* 2000; Huyskens & Bröcker, 2014; Gerogiannis *et al.* 2019), while others assume that the Makrotantalon Unit belongs to the Upper Unit (Dürr, 1986; Bröcker & Franz, 2006; Huet *et al.* 2015), or represents an intermediate position between the main units (Mehl *et al.* 2007). Major arguments for a correlation with the Upper Unit were the tectonic position on top of the Lower Unit, the presumed lack of HP/LT metamorphism and the Cretaceous dates of greenschist-facies rocks (Bröcker & Franz, 2006; Huyskens & Bröcker, 2014), which are unknown from the structurally lower sequences but are typical for low- to medium-grade metamorphic rocks and granitoids on top of the Cycladic Blueschist Unit (e.g. Patzak *et al.* 1994; Martha *et al.* 2016).

Unambiguous evidence for blueschist-facies conditions in the Makrotantalon Unit was interpreted as confirmation of a relationship with the Cycladic Blueschist Unit (Huyskens & Bröcker, 2014). This conclusion was questioned by Huet *et al.* (2015) who reported ^{40}Ar–^{39}Ar phengite dates of ~116 Ma for a glaucophane-garnet schist from the basal part of the Makrotantalon Unit (Fig. 2). Early Cretaceous HP/LT metamorphism has not been observed in the typical Cycladic
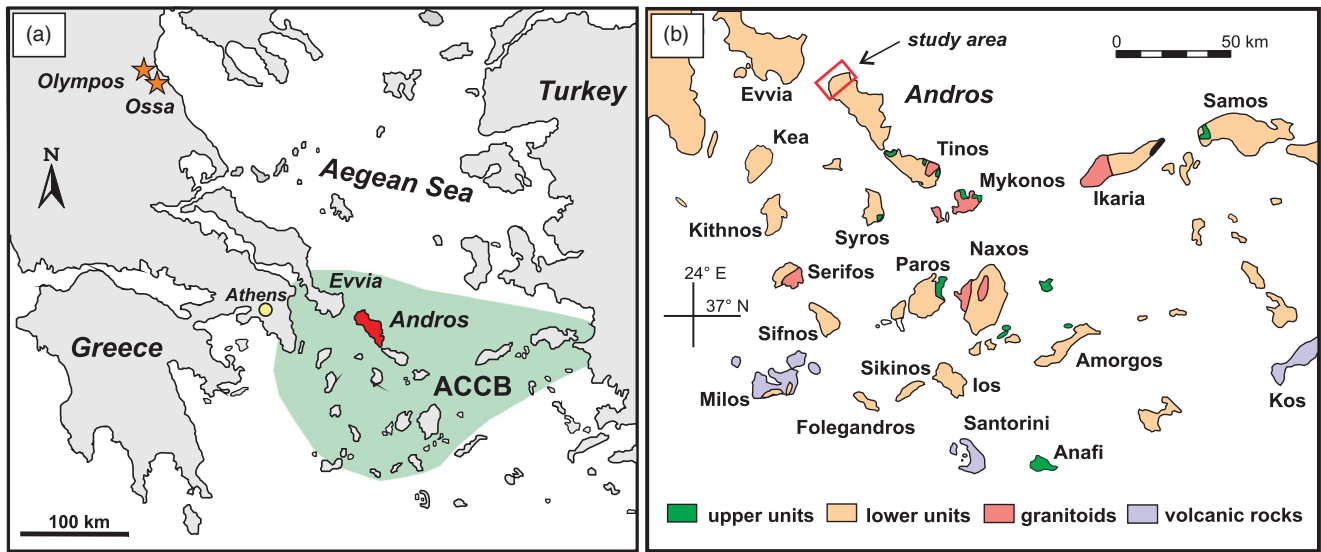
Fig. 1. (Colour online) (a) Geographical overview of the larger study area. ACCB – Attic-Cycladic crystalline belt; stars indicate approximate locations of the Olympos and Ossa tectonic windows. (b) Close-up of the ACCB with schematic overview of the main geological units (modified after Matthews & Schliestedt, 1984). Red rectangle indicates location of the study area that is shown in more detail in Figure 2.
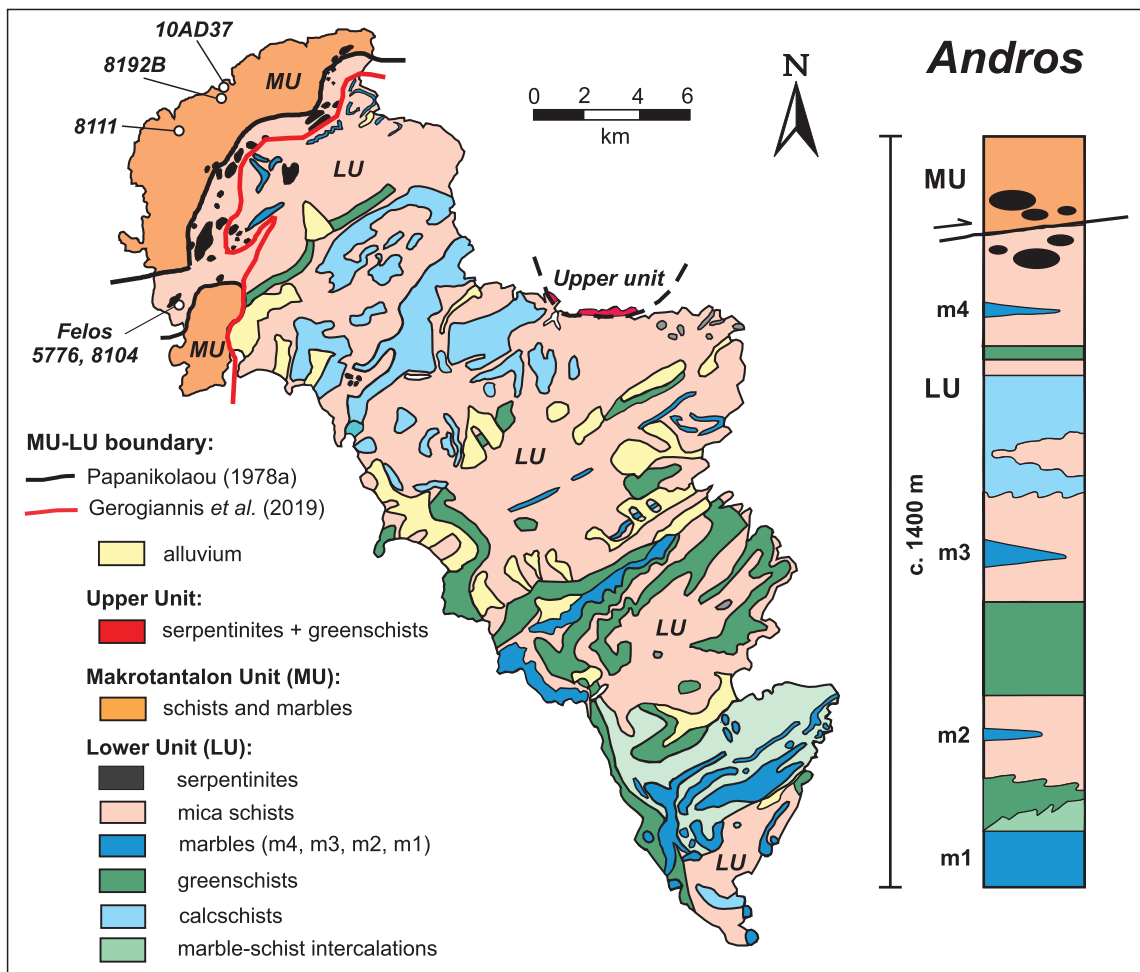
Fig. 2. (Colour online) Simplified geological map and columnar section of Andros (modified after Papanikolaou, 1978*a*).

blueschist sequences, but does occur in the Pelagonian Zone of mainland Greece (e.g. Schermer, 1990; Schermer *et al.* 1990; Lips *et al.* 1998, 1999). Accordingly, Huet *et al.* (2015) suggested a Pelagonian affinity for the Makrotantalon Unit as also indicated by the Cretaceous Rb–Sr dates (~100–90 Ma and ~80–70 Ma) of greenschist-facies rocks from this tectonic unit (Bröcker & Franz, 2006; Huyskens & Bröcker, 2014).

Detailed geological and structural mapping at a scale of 1:15 000 led Gerogiannis *et al.* (2019) to reinterpret the position of the tectonic contact between the Makrotantalon Unit and the Lower Unit and thus the structural position of previously dated samples. On the basis of the new map, Gerogiannis *et al.* (2019) inferred that an epidote-glaucophane schist with a Rb–Sr date of ~45 Ma, originally assigned to the Lower Unit (Bröcker & Franz, 2006), as well as greenschist-facies samples with similar apparent ages from other parts of NW Andros (Huyskens & Bröcker, 2014), belong instead to the Makrotantalon Unit. The revised geological map implies that both Cretaceous and Eocene blueschist-facies rocks are preserved within a distinct subunit of the Cycladic Blueschist Unit. However, this interpretation is still fraught with uncertainty as it is essentially based on the structural assignment of samples collected near a tectonic contact that is challenging to localize in the field owing to the lack of a well-defined shear zone (Mehl *et al.* 2007; Huyskens & Bröcker, 2014). This makes the assignment of samples to the hanging and footwall extremely difficult. The apparent coexistence of blueschist-facies rocks with different ages also raises the question of whether the accuracy of the older dates is compromised by extraneous Ar (e.g. Kelley, 2002; Laurent *et al.* 2017).

This study aims to substantiate the geological significance of the Cretaceous ^{40}Ar–^{39}Ar dates (Huet *et al.* 2015) and to clarify the presumed status of the Makrotantalon Unit as a nappe with Pelagonian origin in the Cycladic Blueschist Unit (Huyskens & Bröcker, 2014; Gerogiannis *et al.* 2019). To achieve these goals, we have dated blueschist-facies rocks from various locations in NW Andros using Rb–Sr geochronology, including two samples from the previously ^{40}Ar–^{39}Ar-dated blueschist area and three samples collected at a greater distance from the tectonic contact in other parts of the Makrotantalon Unit. Using new and published metamorphic ages, the following questions are addressed: Is the Makrotantalon Unit a tectonic slice of the Cycladic Blueschist Unit that records pre-Eocene blueschist metamorphism? Are the Cretaceous ^{40}Ar–^{39}Ar dates of blueschists from the Makrotantalon Unit compromised by either inherited or excess Ar? Did the Makrotantalon Unit undergo separate episodes of HP/LT metamorphism in Cretaceous and Eocene times?

2. Geological setting

The Attic-Cycladic crystalline belt comprises two major tectonic units with different pressure–temperature (*P–T*), time and deformation histories (e.g. Dürr *et al.* 1978; Dürr, 1986; Okrusch & Bröcker, 1990; Ring *et al.* 2010). The structurally higher unit (Upper Unit) is poorly preserved and includes a heterogeneous sequence of unmetamorphosed sediments, Permian to Mesozoic metasediments, Jurassic ophiolites, ophiolites of unknown age, Cretaceous to Palaeogene greenschist-facies rocks, as well as Late Cretaceous granitoids, amphibolites and gneisses (e.g. Patzak *et al.* 1994; Martha *et al.* 2016; Lamont *et al.* 2020a). The Upper Unit lacks evidence for HP/LT metamorphism, which is a key feature of the structurally lower sequences (= Cycladic Blueschist Unit), but its metamorphic rocks could still record subduction-related processes that occurred at a slightly earlier date

and at different *P–T* conditions compared to the Cycladic Blueschist Unit (Lamont *et al.* 2020a).

The Cycladic Blueschist Unit consists of a pre-Alpine crystalline basement and a stack of tectonic units comprising a metamorphosed volcano-sedimentary succession with a polymetamorphic evolution, including an eclogite- to epidote-blueschist-facies event and a greenschist- to upper-amphibolite-facies overprint (e.g. Dürr *et al.* 1978; Dürr, 1986; Papanikolaou, 1987; Okrusch & Bröcker 1990; Ring *et al.* 2010; Philippon *et al.* 2012; Glodny & Ring, 2022). Various geochronological methods, including white mica (K–Ar, Ar–Ar, Rb–Sr), zircon (U–Pb) and garnet (Sm–Nd, Lu–Hf) dating, indicated Eocene (*c.* 55 Ma) to Miocene (*c.* 12 Ma) ages that were interpreted to date HP/LT metamorphism and several stages of lower pressure overprinting, respectively (e.g. Altherr *et al.* 1979, 1982; Wijbrans *et al.* 1990; Bröcker *et al.* 1993; Tomaschek *et al.* 2003; Forster & Lister, 2005; Putlitz *et al.* 2005; Lagos *et al.* 2007; Bröcker *et al.* 2013; Dragovic *et al.* 2015; Cliff *et al.* 2017; Laurent *et al.* 2017; Peillod *et al.* 2017). So far, interpretations suggesting a prolonged Cretaceous–Eocene subduction and exhumation history that are based on U–Pb zircon ages (Bröcker & Enders, 1999; Bröcker & Keasling, 2006) could not be unambiguously confirmed and have been attributed to erroneous linking of protolith ages to metamorphic processes (e.g. Fu *et al.* 2010; Bulle *et al.* 2010). However, metamorphic sole ages of the Tsiknias ophiolite on Tinos also suggest a pre-Eocene stage of subduction and ophiolite obduction at *c.* 74–66 Ma (Lamont *et al.* 2020a).

On Andros, the metamorphic succession can be subdivided into three tectonic units, the Lower Unit, the Makrotantalon Unit and the Upper Unit (Papanikolaou, 1978a,b; Mehl *et al.* 2007; Gerogiannis *et al.* 2019). The Upper Unit only occurs in small outcrops at the NE coast of the island and mainly consists of greenschists and serpentinites, which are separated from the Lower Unit by a flat-lying detachment (Mehl *et al.* 2007). The Lower Unit (up to 1200 m thick) is correlative with the Cycladic blueschist sequences that build up most parts of the neighbouring islands (Syros, Sifnos, Tinos). The main rock types are clastic metasediments, carbonate-rich schists, marbles and various metavolcanic rocks (Papanikolaou, 1978a,b; Gerogiannis *et al.* 2019), which locally are intercalated with manganese-rich quartzites and schists (Reinecke, 1986; Reinecke *et al.* 1985). Ion probe U–Pb zircon dating of felsic metavolcanic rocks yielded Triassic protolith ages (~249–240 Ma; Bröcker & Pidgeon, 2007). Most lithologic units are characterized by greenschist-facies mineral assemblages, but glaucophane-bearing rocks are sporadically preserved (e.g. Papanikolaou, 1978a,b; Mehl *et al.* 2007). Strongly overprinted rocks mostly yielded Miocene Rb–Sr dates (*c.* 23–21 Ma), whereas Eocene Rb–Sr dates (*c.* 44–39 Ma) were reported for the HP/LT event (Bröcker & Franz, 2006; Huyskens & Bröcker, 2014). Estimates of metamorphic conditions indicate temperatures of 450–500 °C and a minimum pressure of 1 GPa for the HP/LT stage, whereas the greenschist-facies overprint occurred at 350–520 °C and 0.5–0.9 GPa (Reinecke, 1986; Bröcker & Franz, 2006).

The Makrotantalon Unit structurally overlies the Lower Unit and is only exposed in the northern part of the island (Fig. 2). The exact position of the inferred tectonic contact between the units is difficult to localize mainly because of intense overprinting by exhumation-related structures (e.g. Papanikolaou, 1978b; Mukhin, 1996; Mehl *et al.* 2007; Huyskens & Bröcker, 2014; Gerogiannis *et al.* 2019). Huyskens & Bröcker (2014) considered a discontinuous serpentinite belt that extends through NW Andros (Papanikolaou, 1978a,b) as a suitable marker of the shear

zone, but a clear assignment of the ultramafic rocks to one of the two nappes is difficult. From lithostratigraphic observations, Papanikolaou (1978b) interpreted the ultramafic rocks as a distinct olistostromatic horizon within the Lower Unit, placing the tectonic contact above the serpentinite belt. T. A. Shin (unpub. Master's thesis, Univ. Texas at Austin, 2014) suggested that the serpentinites are part of the Makrotantalon Unit, inferring a tectonic contact below the ultramafic rocks. In contrast, Gerogiannis *et al.* (2019) concluded that the serpentinite bodies are exposed at different structural levels within both tectonic units and thus cannot be used for delineating the nappe contact. These authors used lithological differences and the presence of mylonitic rocks for mapping of the boundary between the units. Eocene dates (~40 Ma; Rb–Sr internal isochrons) recorded in samples collected close to the presumed shear zone were interpreted as the lower time limit for tectonic juxtaposition (Huyskens & Bröcker, 2014). Permian fossils in dolomitic marbles of the Makrotantalon Unit and Triassic or younger zircon protolith or maximum sedimentation ages of the Lower Unit support the interpretation that the units were originally separated by a thrust zone (Papanikolaou, 1978a,b; Huyskens & Bröcker, 2014). Other studies suggested the existence of a presumably low-angle normal fault with top-to-the-NE kinematics, proposed the reactivation of an earlier thrust fault as a normal fault or questioned whether a tectonic contact exists at all (Dürr, 1986; Avigad & Garfunkel, 1991; Avigad *et al.* 1997; Bröcker & Franz, 2006; Bröcker & Pidgeon, 2007; Mehl *et al.* 2007; Huyskens & Bröcker, 2014; Huet *et al.* 2015). Gerogiannis *et al.* (2019) found no structural evidence for reactivation of a thrust as a low-angle normal fault but inferred that the original contact was folded during exhumation and transposed by NE-directed shearing. Gerogiannis *et al.* (2019) also reasoned that structural data from Andros are more consistent with NE- than with SW-directed ductile extrusion, as suggested for other parts of the Cyclades (e.g. Doutsos *et al.* 1993; Xypolias *et al.* 2003, 2012; Aravadinou *et al.* 2016; Gerogiannis & Xypolias, 2017).

The Makrotantalon Unit (up to 600 m thick) mainly consists of clastic metasedimentary rocks, dolomite marbles and minor metabasic schists (Papanikolaou, 1978a,b; Gerogiannis *et al.* 2019). Glaucophane-bearing rocks are locally preserved, but greenschist-facies mineral assemblages are more common (Mukhin, 1996; Huyskens & Bröcker, 2014; Gerogiannis *et al.* 2019). For blueschist-facies rocks, multi-equilibrium thermobarometry indicates peak metamorphic conditions of 550 °C and 1.85 GPa (Huet *et al.* 2015), which are largely consistent with *P–T* estimates for Eocene HP/LT rocks of the Cycladic Blueschist Unit on neighbouring islands (e.g. Parra *et al.* 2002; Philippon *et al.* 2012; Laurent *et al.* 2018; Lamont *et al.* 2020b; Glodny & Ring, 2022 and references therein). Greenschist-facies rocks of the Makrotantalon Unit record *P–T* conditions of 350–455 °C and 0.41–0.54 GPa (Bröcker & Franz, 2006). Single phengite grains of a glaucophane-garnet schist from the basal part of the Makrotantalon Unit yielded ^{40}Ar–^{39}Ar plateau dates of ~116 Ma. White mica geochronology of greenschist-facies rocks produced Rb–Sr dates between *c.* 104 Ma and *c.* 21 Ma, which were interpreted to document distinct metamorphic episodes in the Cretaceous (*c.* 100–90 Ma and *c.* 80–70 Ma) and Miocene (*c.* 24–21 Ma) periods (Bröcker & Franz, 2006). The new map by Gerogiannis *et al.* (2019) indicates that a HP/LT rock with a Rb–Sr date of *c.* 45 Ma, originally interpreted as part of the Lower Unit (Bröcker & Franz, 2006), was instead collected in the Makrotantalon Unit, suggesting an even more complex polymetamorphic history.

On a regional scale, the Makrotantalon Unit can be correlated with the HP/LT nappe stack exposed in southern Evia where the Cycladic Blueschist Unit comprises three subunits (Ochi, Styra and Tsaki; e.g. Papanikolaou, 1978b; Katzir *et al.* 2000; Shaked *et al.* 2000). Gerogiannis *et al.* (2019) interpreted the Makrotantalon Unit as the lateral equivalent of the Ochi nappe on Evia (as also suggested by Papanikolaou, 2013), because of its identical structural position, lithological similarities and matching tectonometamorphic history. In contrast, Huyskens & Bröcker (2014) questioned a clear relationship to a specific tectonic slice on Evia and considered the possibility that the Makrotantalon Unit may represent a distinct subunit with similarities to the tectonic-metamorphic history of the south Evia nappe stack.

3. Methods

Mineral compositions were determined with a JEOL 8530F electron microprobe (EMP). Natural and synthetic mineral standards were used for calibration. Operating conditions were 15 kV accelerating voltage, 5 nA electron beam current and a spot size of 5 µm. Counting times were 5 s on the peak and 2 s on the background. Analytical data are summarized in online Supplementary Material Table S1.

For preparation of mineral separates for Rb–Sr analysis, hand specimens were cut into ~10–20 mm thick rock slabs. Weathered crusts were removed, and fresh material was first crushed in a steel mortar and then its grain size was further reduced by repeated short grinding intervals in a tungsten carbide shatterbox. Following sieving, minerals were either enriched by adherence to a piece of paper or with a Frantz magnetic separator, followed by handpicking under the stereo microscope. Before dissolution, mineral concentrates were repeatedly rinsed in deionized H_2O and in ethanol. Mineral separates (phengite: 2–12 mg; mostly <8 mg; epidote: 1–2 mg) and whole-rock powders (~100 mg) were mixed with ^{87}Rb–^{84}Sr spike in Teflon vials and dissolved in HF–HNO_3 (5:1) on a hot plate overnight. After complete evaporation, 6 N HCl was added to the residue. This mixture was again homogenized on a hot plate overnight. After a second evaporation to dryness, Rb and Sr were separated by standard ion exchange procedures (AG 50W-X8 resin) on quartz glass columns using 2.5 N HCl as the eluent.

For mass-spectrometric analysis, Sr was loaded with TaF_5 on W filaments and measured in static mode using a Thermo Finnigan Triton thermal ionization mass spectrometer (TIMS). During the two analytical sessions of this study, the NIST SRM 987 reference material yielded $^{87}Sr/^{86}Sr$ values of 0.710292 ± 0.000015 (2σ; n = 10) and 0.710301 ± 0.000012 (2σ; n = 9), respectively. The $^{87}Sr/^{86}Sr$ values of samples are reported relative to 0.710248 for the SRM 987. Correction for mass fractionation is based on $^{86}Sr/^{88}Sr = 0.1194$ using the exponential law. Data were corrected for total procedural blanks of 10 pg for Rb and 20 pg for Sr.

Rubidium concentrations were determined by isotope dilution with a multiple-collector inductively coupled plasma mass spectrometer (MC-ICP-MS) (Thermo Neptune Plus), using admixed Zr to correct for the instrumental mass bias (Nebel *et al.* 2005). The external reproducibility on the Rb/Sr of samples was estimated from the repeated analysis of optimally spiked standard solutions and samples, i.e. 0.1–0.2 %. This uncertainty was then multiplied by an error magnification factor to account for over- or underspiking (e.g. Stracke *et al.* 2014). For isochron calculations, $^{87}Sr/^{86}Sr$ values were assigned external 2σ uncertainties of 0.005 %. Data

evaluation, age calculation and presentation in diagrams is based on Isoplot/Ex 4.15 (Ludwig, 2012) using the [87]Rb decay constant of Villa *et al.* (2015). Isochron dates are reported with Model 1 solutions at the 95 % confidence level.

4. Samples

Five samples were selected for Rb–Sr geochronology. Sampling locations are illustrated in Figure 2, and GPS coordinates are reported in Table 1. Field images are shown in Figure 3. Photomicrographs are depicted in Figure 4 and online Supplementary Material Figure S1.

Samples 5776 and 8104 (Fig. 4a, b) are strongly foliated and partially folded garnet-glaucophane schists from the Fellos area that were collected from the same lithological horizon in close vicinity to each other. The mineral assemblage mainly consists of garnet, glaucophane, phengite, quartz and rutile. Zircon is a typical accessory phase. Garnet occurs as porphyroclasts and is often strongly fragmented. Iron oxide-stained garnet is common. Heterogeneously distributed white mica and sodic amphibole define the foliation. Glaucophane is generally well-preserved and mostly lacks obvious signs of retrogression. Titanite, chlorite and a brown phyllosilicate (biotite or oxychlorite) document variable degrees of lower pressure overprinting.

Sample 8111 is a weakly crenulated epidote-glaucophane schist that was collected near the lighthouse at Fasa (Figs 2, 4c). This rock mainly consists of epidote, glaucophane and phengite. Quartz, titanite, apatite, tourmaline and opaque phases occur in minor or accessory modal quantities. Titanite was stable at peak conditions. Chlorite and albite are secondary.

Samples 10AD37 and 8192B are epidote-glaucophane schists from the area NE of Kalivari (Figs 2, 4d, e). The mineral assemblages are similar to that of sample 8111, but the rocks are more crenulated. In sample 10AD37, glaucophane has been partially replaced by a more calcic amphibole.

For details of the structural inventory and deformation history of NW Andros see Gerogiannis *et al.* (2019).

5. Results

5.a. Mineral chemistry

To characterize the white mica populations and to identify mixed populations, polished thin-sections were prepared from splits of the phengite separates that were used for white mica isotopic analyses, with the basal plane of mica plates positioned parallel to the surface of the glass slide. This orientation allowed systematic and representative EMP analysis of core and near rim compositions, and for each sample, phengite from different sieve fractions was analysed (~25–30 core–rim pairs each; online Supplementary Material Table S1). White mica compositions were also determined *in situ* in polished thin-sections. The Si-content was used as a proxy to evaluate inter- and intragrain compositional variability and inferred relative pressure differences (Massonne & Schreyer, 1987). Results are shown in Figures 5 and 6.

Most white mica populations are paragonite-free and only consist of phengite. Small amounts of paragonite were only recognized in sample 8104. Separated grains are characterized by rather homogeneous compositions, and no difference between different grain-size fractions is evident (Fig. 5; online Supplementary Material Table S1). Most of these grains show only slight zoning of Si-values without a uniform trend (Fig. 6a).

Two generations of phengite were recognized in the *in situ* data of samples 5776 and 8104, which comprise crystals with Si-values of 3.43–3.55 and 3.22–3.34, respectively, and also differ in their X_{Na}-values (<0.1 and 0.11–0.20; Figs 5a, d, 6b; online Supplementary Material Table S1). The dataset of separated grains from these samples almost completely comprises phengite of the low-Si group (3.23–3.33), which is characterized by elevated Na_2O concentrations (0.8–1.6 wt %) and lower K_2O contents (8.8–10.8 wt %) compared to the high-Si phengites. The X_{Na} (Na/(Na + K + Ca)) value is typically 0.11–0.21, and X_{Mg} (Mg/(Mg + Fe + Mn)) values are in the 0.63–0.73 range.

White mica of samples 8111 and 8192B show little intra- and inter-sample variations and are characterized by Si-values of 3.37–3.55 and 3.38–3.59, respectively, without compositional differences between isolated and *in situ* analyses (Fig. 5g–l). The X_{Mg} value is in the range from 0.40 to 0.69 and X_{Na} is <0.1. *In situ* analysed phengite of sample 10AD37 has similar compositional characteristics (Si: 3.44–3.57; X_{Mg}: 0.48–0.71; X_{Na}: <0.1).

Most amphiboles are glaucophane, but the compositional range extends slightly into the ferro-glaucophane and magnesio-riebeckite fields (Fig. 7). Two compositional groups can be distinguished. Sodic amphiboles of samples 5776 and 8104 are characterized by X_{Mg} (Mg/(Mg + Fe^{2+})) of 0.47–0.57 and X_{Fe3+} ((Fe^{3+}/(Fe^{3+} + Al^{VI})) of 0.07–0.17. In the other samples, X_{Mg} and X_{Fe3+} are 0.59–0.86 and 0.29–0.6, respectively. Epidotes have pistacite values (X_{Fe3+} = Fe^{3+}/(Fe^{3+} + Al)) of 0.25–0.31. The concentrations of Cr_2O_3 reach up to 0.33 wt % but are mostly <0.1 wt %. The MnO contents are in the range of 0.16–0.79 wt %.

5.b. Rb–Sr geochronology

The Rb–Sr isochrons are based on different size fractions obtained by sieving of crushed rock. Coarser sieve fractions probably contain mostly grains that were originally coarse. Fine sieve fractions probably contain a mix of originally fine grains and broken fragments of originally coarser grains. In the case of fully equilibrated rocks, this will not affect the isochron age. However, complexities can arise from inheritance and disequilibria, which can often be identified by the systematic deviation of the smallest or largest sieve size fractions from the regression line.

Analytical data are summarized in Table 1 and shown in Figure 8. Phengite grains of samples 5776 and 8104 have relatively high Sr concentrations of ~120–170 ppm, whereas white mica of the other samples is characterized by Sr contents of <10–28 ppm. Epidote splits of sample 8111 have relatively high Rb concentrations (15–18 ppm) indicating imperfect purification or the presence of white mica inclusions. This has no significant effect on the isochron plots because of the high Sr concentrations of the epidotes (1400–1500 ppm).

Apparent ages of the garnet-glaucophane schists 5776 and 8104 are based on a set of different sieve fractions of phengite. In both cases, linear regression indicates strong scatter. For sample 5776, the <425 µm grain-size fractions indicate an apparent age of 21.0 ± 3.2 Ma (Mean Square Weighted Deviation, MSWD = 9.7; Fig. 8a). Eight <355 µm grain-size fractions of sample 8104 mica yielded a Rb–Sr date of 15.1 ± 5.9 Ma (MSWD = 14; Fig. 8a). The excluded two larger grain-size fractions of samples 5776 and 8104 plot along a 117 Ma reference line (Fig. 8a). For sample 8111, 11 data points were determined, representing different sieve fractions of phengite (9x) and epidote (2x). Excluding the <200 µm phengite splits results in a straight-line fit with a Rb–Sr date of 121 ± 5 Ma (MSWD = 585; Fig. 8b). White mica (4x) and epidote (1x) aliquots

Table 1. Rb–Sr isotope data of blueschist-facies rocks from the Makrotantalon Unit

Sample	Mineral	Size fraction (µm)	ppm Rb	ppm Sr	$^{87}Rb/^{86}Sr$	$2\sigma^{\star}$	$^{87}Sr/^{86}Sr$	$2\sigma_{m}$
5776	**Garnet-glaucophane schist; GPS coordinates: 37° 54.388 N, 024° 42.520 E**							
	phengite	A (>500)	332	152	6.338	0.010	0.730609	0.000007
	phengite	B (500–425)	334	144	6.747	0.011	0.731163	0.000006
	phengite	C (425–355)	333	156	6.182	0.010	0.730185	0.000007
	phengite	D (355–300)	339	155	6.341	0.010	0.730277	0.000007
	phengite	F (300–250)	342	152	6.514	0.010	0.730230	0.000006
	phengite	H (250–180)	349	138	7.364	0.011	0.730609	0.000007
	phengite	L (180–125)	326	85.7	11.04	0.02	0.731612	0.000007
8104	**Garnet-glaucophane schist; GPS coordinates: 37° 54.382 N, 024° 42.510 E**							
	phengite	B (500–425)	310	158	5.693	0.009	0.729504	0.000006
	phengite	C (425–355)	313	162	5.609	0.009	0.729335	0.000007
	phengite	D (355–300)	320	165	5.640	0.009	0.729073	0.000007
	phengite	F (300–250)	329	165	5.789	0.022	0.729025	0.000006
	phengite	H (250–180)	344	158	6.325	0.009	0.729216	0.000006
	phengite	L (180–125)	351	140	7.286	0.048	0.729479	0.000008
	phengite	F (300–250)	355	166	6.203	0.015	0.729185	0.000006
	phengite	G (250–200)	326	147	6.417	0.015	0.729115	0.000006
	phengite	J (200–160)	320	132	7.047	0.017	0.729247	0.000006
	phengite	M (160–125)	320	118	7.890	0.018	0.729496	0.000006
10AD37	**Epidote-glaucophane schist; GPS coordinates: 37° 58.559 N, 024° 43.602 E**							
	phengite	E (355–250)	138	24.5	16.27	0.02	0.714295	0.000008
	phengite	E (355–250)	148	6.34	67.81	0.09	0.744263	0.000016
	phengite	H (250–180)	151	3.27	134.5	0.2	0.781041	0.000009
	phengite	L (180–125)	148	5.75	74.67	0.10	0.746192	0.000009
	epidote	L (180–125)	9.23	1180	0.02253	0.00160	0.705784	0.000010
	whole rock†	>500	72.9	408	0.5175	0.0054	0.705839	0.000006
	whole rock†	>500	74.6	410	0.5268	0.0066	0.705833	0.000006
8111	**Epidote-glaucophane schist; GPS coordinates: 37° 57.962 N, 024° 42.170 E**							
	phengite	E (355–250)	208	27.2	22.17	0.06	0.746278	0.000008
	phengite	H (250–180)	209	24.4	24.87	0.05	0.748943	0.000013
	phengite	L (180–125)	217	17.1	36.77	0.17	0.748868	0.000011
	phengite	D (355–300)	205	27.5	21.59	0.06	0.745091	0.000008
	phengite	F (300–250)	208	28.0	21.60	0.05	0.744070	0.000008
	phengite	G (250–200)	209	24.2	25.05	0.05	0.747840	0.000008
	phengite	I (200–180)	212	24.0	25.62	0.06	0.747390	0.000008
	phengite	K (180–160)	212	19.5	31.60	0.07	0.749472	0.000009
	phengite	M (160–125)	215	15.6	40.06	0.11	0.749182	0.000008
	epidote	H (250–180)	18.1	1430	0.03654	0.00016	0.707487	0.000005
	epidote	L (180–125)	14.8	1490	0.02877	0.00008	0.707510	0.000006
8192B	**Epidote-glaucophane schist; GPS coordinates: 37° 58.277 N, 024° 43.562 E**							
	phengite	D (355–300)	188	5.93	92.32	0.38	0.767484	0.000013
	phengite	F (300–250)	188	5.05	108.3	0.3	0.779448	0.000014
	phengite	G (250–200)	192	7.15	77.92	0.18	0.756108	0.000010

(Continued)

Table 1. *(Continued)*

Sample	Mineral	Size fraction (µm)	ppm Rb	ppm Sr	$^{87}Rb/^{86}Sr$	$2\sigma^*$	$^{87}Sr/^{86}Sr$	$2\sigma_m$
	phengite	J (200–160)	195	6.86	82.82	0.20	0.757905	0.000015
	phengite	M (160–125)	200	6.08	95.90	0.22	0.763593	0.000016
	epidote	G (250–200)	6.58	885	0.02151	0.00007	0.707989	0.000005
	epidote	J (200–160)	5.72	890	0.0186	0.0001	0.708008	0.000006
	epidote	M (160–125)	4.69	913	0.0149	0.0001	0.708060	0.000005
	whole rock†	>355	103	208	1.426	0.005	0.708627	0.000006
	whole rock†	>355	103	208	1.438	0.013	0.708613	0.000007

*The external reproducibility (2σ) of $^{87}Rb/^{86}Sr$ was estimated from the repeated analysis of optimally spiked standard solutions and samples, and includes an error magnification for under- or overspiking. The $2\sigma_m$ uncertainties on $^{87}Sr/^{86}Sr$ represent the internal analysis statistics (2 standard errors). For age calculations, all $^{87}Sr/^{86}Sr$ values were assigned an uncertainty of 0.005 % (2σ).
†Whole-rock powders were prepared from different grain-size fractions, not from a full sample.
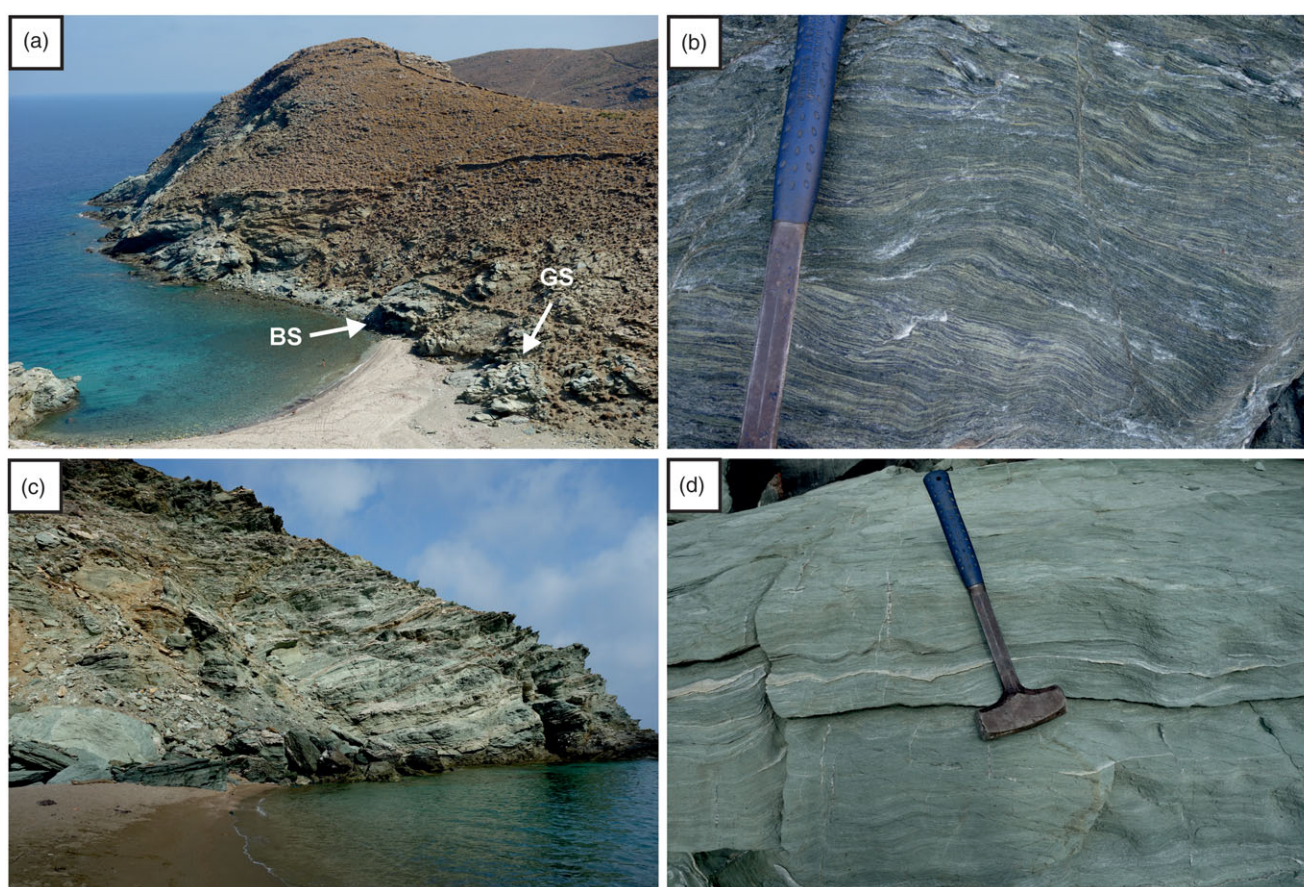

Fig. 3. (Colour online) Field images from the Makrotantalon Unit. (a) Overview of the outcrop at Mikri Peza; BS – blueschist; GS – greenschist. (b) Close-up of epidote-glaucophane schist from this outcrop locality, indicated in (a) with arrow 'BS'. (c, d) Greenschist-facies rock sequences forming most parts of the peninsula shown in (a) as exposed in the next bay (Meghali Peza). Hammer for scale in (b) and (d) is 30 cm in length.

of sample 10AD37 yielded a Rb–Sr date of 39.9 ± 2.0 Ma (MSWD = 727), and of 39.9 ± 1.1 Ma (MSWD = 436; Fig. 8c), if two whole-rock analyses are included. In the case of sample 8192B, alignment of data points representing sized fractions of phengite (5x) and epidote (3x) yielded a Rb–Sr date of 44.3 ± 2.2 Ma (MSWD = 1103). Inclusion of the whole-rock data points into the linear regression gives an apparent age of 44.3 ± 1.8 Ma (MSWD = 857; Fig. 8d).

6. Discussion

Previous studies indicated that the Makrotantalon Unit records a complex polymetamorphic history, including an Early Cretaceous blueschist-facies event, a Late Cretaceous greenschist- to amphibolite-facies episode, an Eocene HP/LT metamorphic event and a Miocene greenschist-facies overprint (Bröcker & Franz 2006; Huyskens & Bröcker, 2014; Huet *et al.* 2015; Gerogiannis *et al.* 2019). In the following, we critically evaluate interpretations
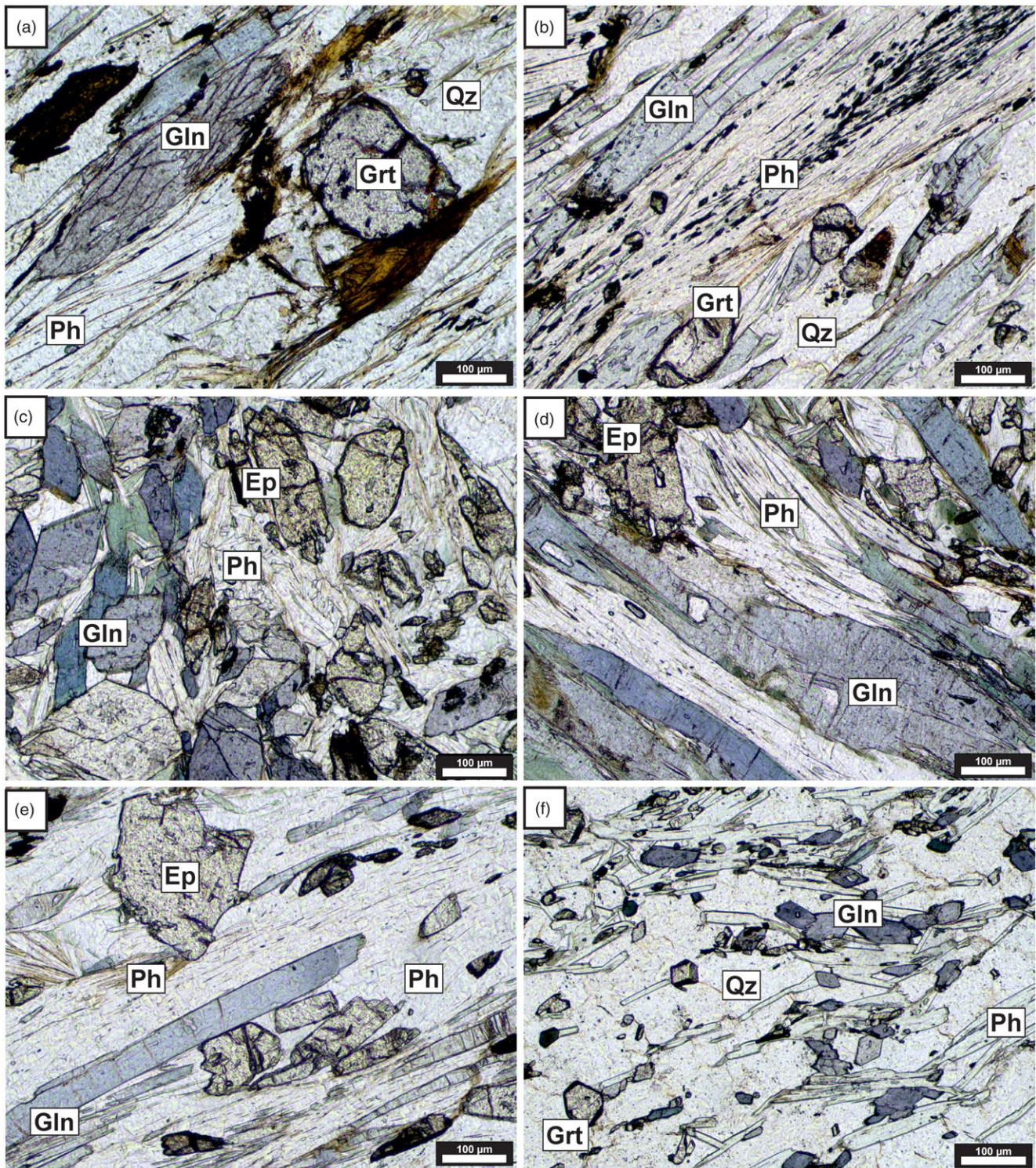
Fig. 4. (Colour online) Thin-section photomicrographs of blueschist-facies samples from the Makrotantalon Unit that were used for Rb–Sr geochronology (plane-polarized light). (a) Sample 5776. (b) Sample 8104. (c) Sample 8111. (d) Sample 10AD37. (e) Sample 8192B. (f) Sample 1453, dated by Bröcker & Franz (2006) and originally assigned to the Lower Unit. Ph – phengite; Ep – epidote; Gln – glaucophane; Qz – quartz; Grt – garnet. Scale bar is 100 µm across.

suggesting that the Makrotantalon Unit was affected by two blueschist-facies events at different times (Gerogiannis *et al.* 2019) using new and existing geochronological data.

Peak metamorphic temperatures of the Makrotantalon blueschists (~550 °C; Huet *et al.* 2015) are close to the commonly cited empirical bulk closure temperature for the Rb–Sr isotope system of white mica (~500–550 °C; e.g. Purdy & Jäger, 1976; von Blanckenburg *et al.* 1989). This suggests that the new mineral isochron dates were not significantly affected by cooling, but instead indicate the time of (re)crystallization or subsequent disturbance by infiltrating fluids. The similarity with the Ar–Ar white mica dates (closure temperature ~400–440 °C, e.g. Harrison *et al.*
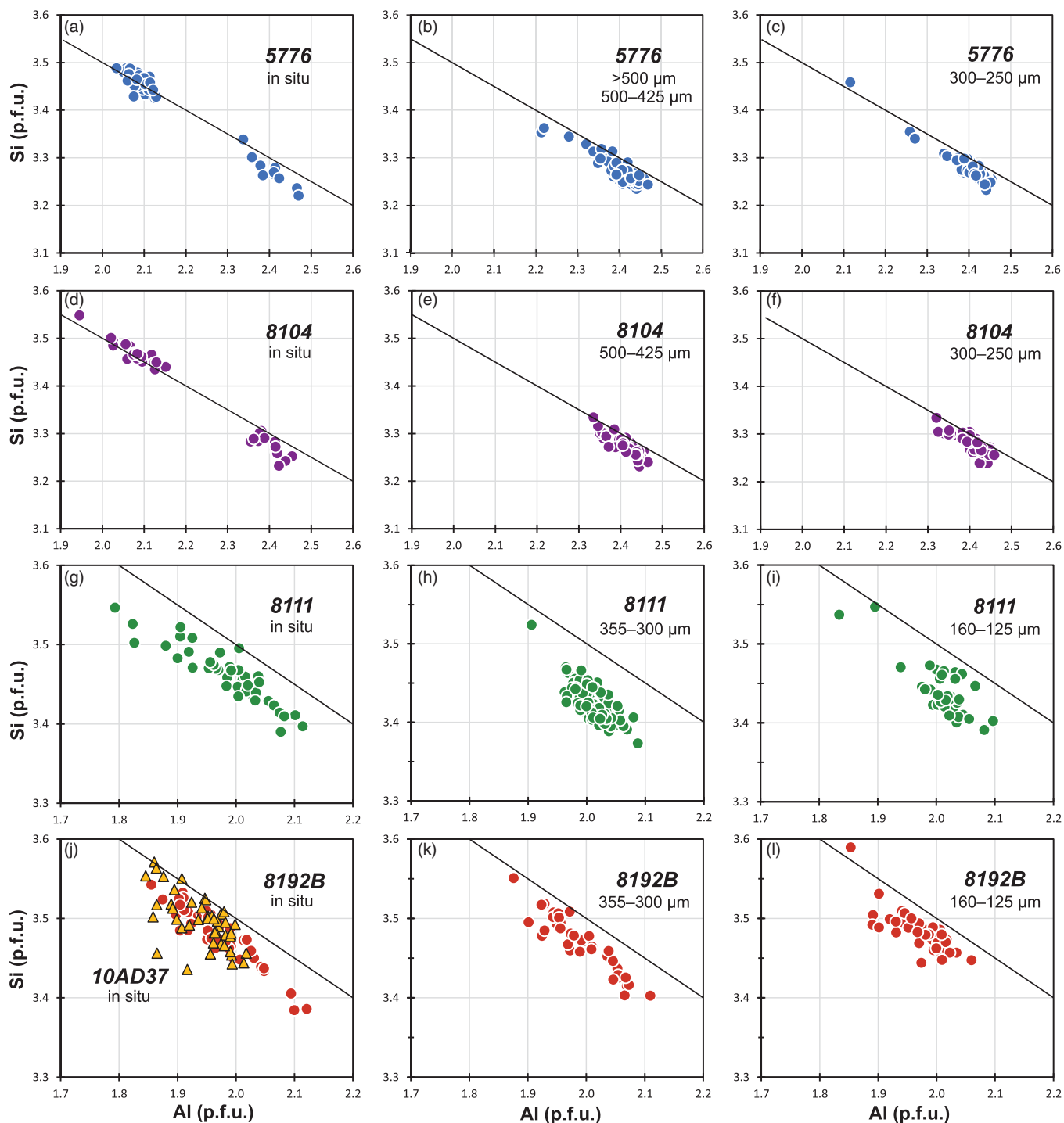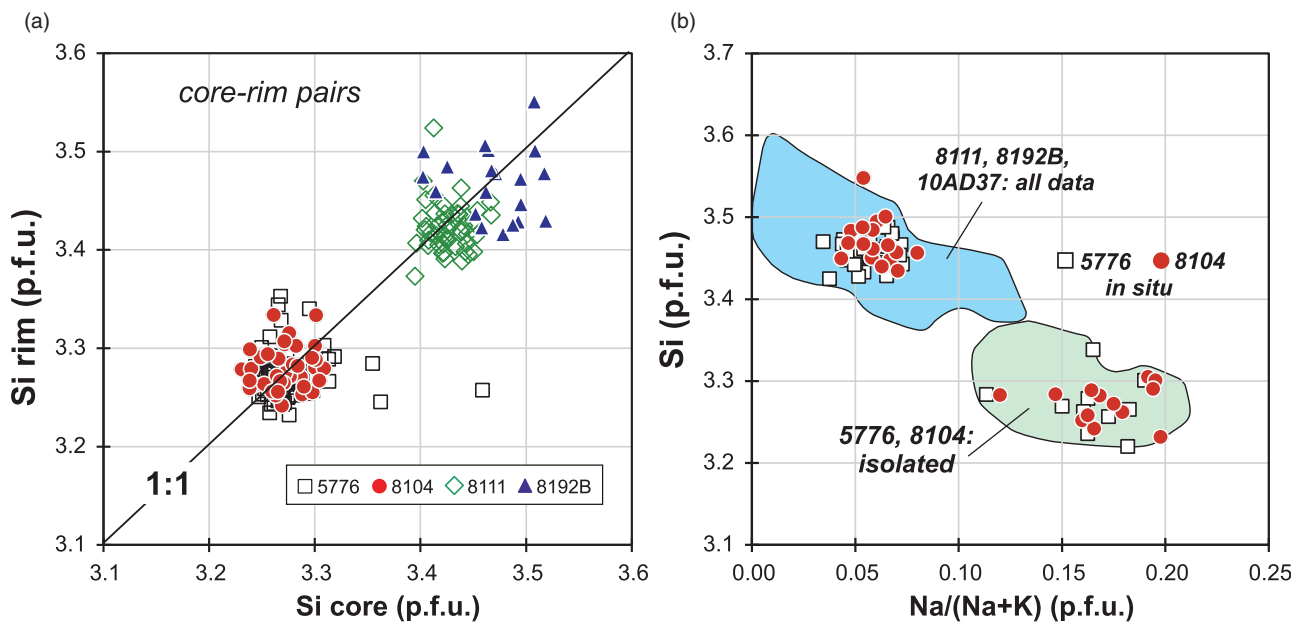
Fig. 5. (Colour online) Si versus Al diagrams (atoms per formula unit) for white mica of Makrotantalon samples representing different grain-size fractions of separated (isolated) grains and *in situ* analyses. The lines indicate a compositional trend from muscovite to aluminoceladonite.

2009; Scharf *et al.* 2016) indicates fast exhumation and is consistent with this interpretation.

The Rb–Sr regressions yielded high MSWD values for all studied samples. This value provides a goodness-of-fit parameter for data points plotting along the regression line, which defines the age-dependent slope of the isochron. In the present case, these values cannot be further optimized by rejection of individual data points from the regression. This would only be justified in the case of obvious disequilibrium. In general, the MSWD is controlled by a combination of geological factors and analytical precision. The scatter of data points beyond analytical error (leading to large MSWD values) is a common issue affecting incompletely recrystallized polymetamorphic or polydeformed samples (e.g. Halama *et al.* 2018). Furthermore, for a given amount of real geologic scatter in Andros Rb–Sr regressions, the MSWD will be higher when the analytical uncertainties are smaller. In TIMS studies, the ^{87}Rb/^{86}Sr values are often reported with 1–1.5 % uncertainty, which is estimated from replicate analyses of unspiked or spiked samples

Fig. 6. (Colour online) White mica compositions (atoms per formula unit) of Makrotantalon samples. (a) Si rim versus Si core; 1:1 reference line indicates no zoning. (b) Si versus X_{Na} diagram.
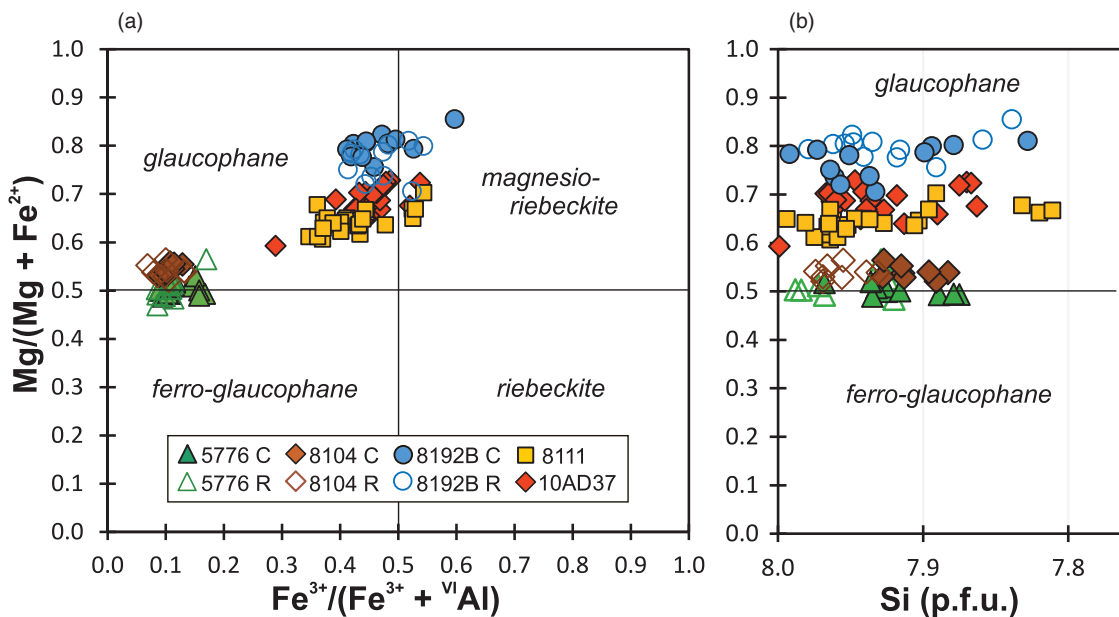

Fig. 7. (Colour online) Amphibole classification diagrams (atoms per formula unit, based on Locock, 2014) of Makrotantalon samples. (a) Mg/(Mg + Fe^{2+}) versus Fe^{3+}/(Fe^{3+} + ^{VI}Al) diagram. (b) Mg/(Mg + Fe^{2+}) versus Si (Leake *et al.* 1997). C – core; R – rim.

or reference materials. In contrast, MC-ICP-MS allows a more precise determination of the Rb isotope ratio by correcting the instrumental mass bias using admixed Zr, leading to a much better reproducibility of the measurements (e.g. Nebel *et al.* 2005). For example, the uncertainty of the ^{87}Rb/^{86}Sr phengite data (MC-ICP-MS) of samples 8111, 10AD37 and 8192B is mostly <0.4 %, resulting in MSWD values of 585, 436 and 857, respectively. In contrast, a more TIMS-typical uncertainty of 1 % on the ^{87}Rb/^{86}Sr ratios would result in MSWD values of 36, 41 and 89, respectively. These values are still indicative of errorchrons (e.g. Wendt & Carl, 1991), but a high MSWD is not a priori an indication of

geological irrelevance (e.g. Kalsbeek & Hansen, 1989; Halama *et al.* 2018). Since the apparent ages coincide with existing Ar–Ar and Rb–Sr dates for similar rocks from the study area, the new results are considered geologically meaningful, closely approximating the true metamorphic ages.

6.a. Cretaceous HP/LT metamorphism in the Makrotantalon Unit?

In the Fellos area (Fig. 2), HP/LT rocks are exposed below a serpentinite body that extends over several hundred metres along a
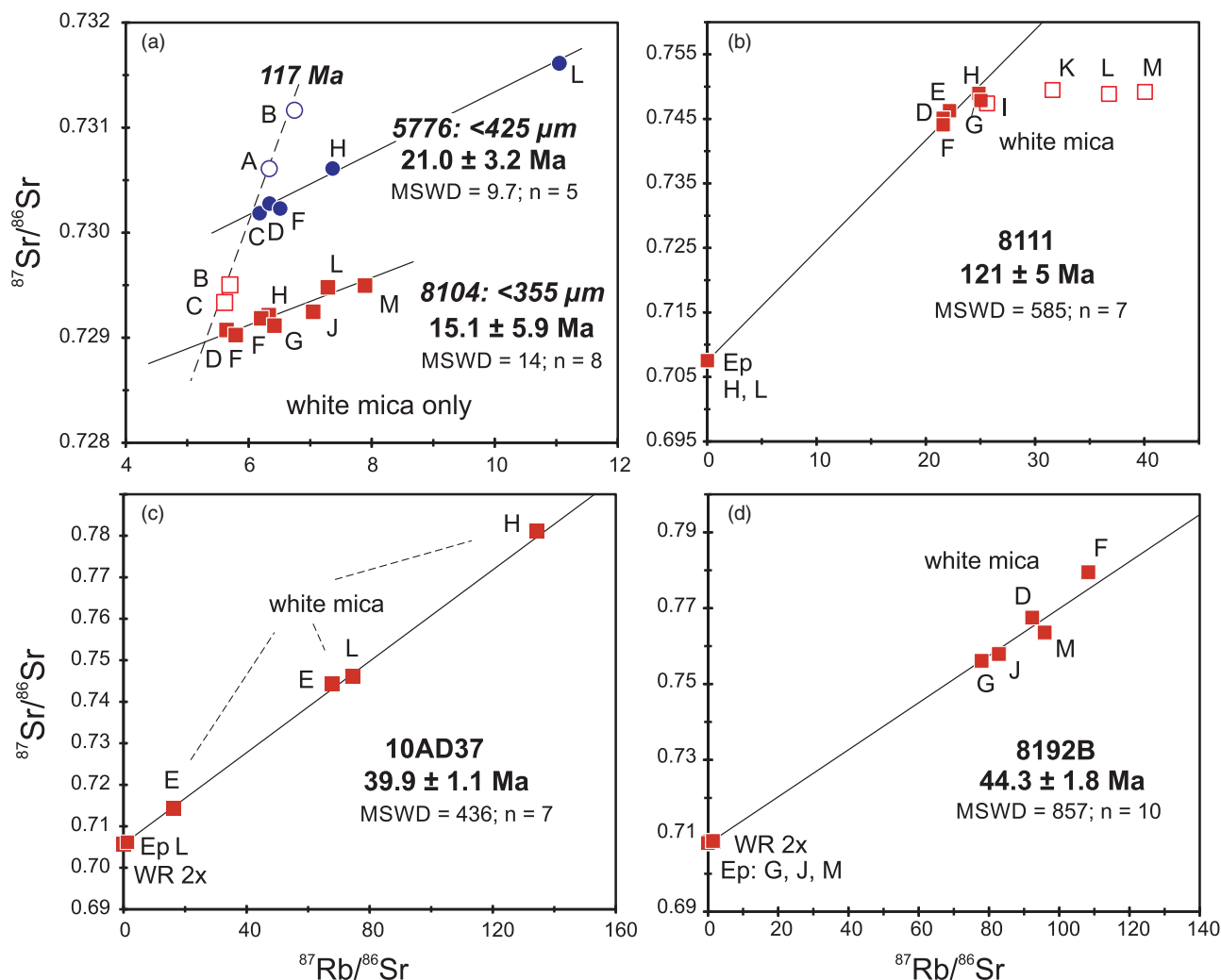
Fig. 8. (Colour online) Rb–Sr isochron diagrams for blueschist-facies samples from the Makrotantalon Unit. Ph – phengite; Ep – epidote. Uncertainties are smaller than symbol size. A, B, C, etc. refer to sieved grain-size fractions indicated in Table 1.

mountain ridge (Mukhin, 1996). Huyskens & Bröcker (2014) interpreted the serpentinite as a lithological marker of the tectonic contact between the Makrotantalon and the Lower Unit, whereas Xypolias *et al.* (2018) argued that the contact is located a few hundred metres beneath the serpentinite. An epidote-glaucophane schist collected in the lower part of the metasedimentary succession below the serpentinite body yielded an Eocene Rb–Sr date (45.7 ± 3.2 Ma; Bröcker & Franz, 2006). At a similar lithostratigraphic position elsewhere on the island, relics of Na-amphibole are also sporadically preserved in strongly overprinted rocks. Most of these greenschist-facies samples yielded white mica Rb–Sr dates of ~40 Ma (Huyskens & Bröcker, 2014). The Eocene dates were interpreted as a legacy of the HP/LT event recorded in the Cycladic Blueschist Unit, and the sampling locations were therefore considered to belong to the Lower Unit (Huyskens & Bröcker, 2014).

Huyskens & Bröcker (2014) reported clear evidence for blueschist-facies metamorphism from other locations in the Makrotantalon Unit but did not find suitable glaucophane-bearing samples for white mica geochronology that could unambiguously be assigned to this nappe. These authors assumed that both the Makrotantalon Unit and the Lower Unit were affected

by a single blueschist-facies event in the Eocene and concluded that the Makrotantalon Unit is a distinct tectonic subunit of the Cycladic Blueschist Unit. This interpretation was challenged by ^{40}Ar–^{39}Ar single phengite dating of a glaucophane-garnet schist from a higher lithostratigraphic position in the Fellos succession that yielded Cretaceous dates (117.2 ± 1.8 Ma, 115.6 ± 1.9 Ma, 105.9 ± 1.7 Ma; Huet *et al.* 2015). The youngest date overlaps with apparent Rb–Sr ages of greenschist-facies rocks (104.6 ± 3.8 Ma and 103.9 ± 1.3 Ma; Bröcker & Franz, 2006), which was interpreted as an indication that a contamination with excess Ar is insignificant and that the ^{40}Ar–^{39}Ar dates represent geologically meaningful crystallization ages. However, this argument is not fully convincing because the ^{40}Ar–^{39}Ar and Rb–Sr dates were determined on rocks having different metamorphic histories.

In the Fellos area, garnet-glaucophane schists occur within a sequence of siliciclastic metasedimentary rocks. Huet *et al.* (2015) reported that the Ar–Ar-dated sample was collected within the serpentinites. Our field observations indicate that such rocks only occur below the serpentinite, but judging from their sample description, the Rb–Sr dated samples 5776 and 8104 correspond to the same rock type that yielded the Cretaceous ^{40}Ar–^{39}Ar dates.

White mica geochronology of rocks with a complex, multi-phase tectonometamorphic evolution is often compromised by incomplete resetting of the isotopic system or the presence of different mica generations (e.g. Bröcker *et al.* 2013; Kurzawa *et al.* 2017). The phengite population of the Ar–Ar-dated sample included two compositional groups with Si-values of ~3.4 and ~3.2, respectively, that were recognized both *in situ* and in isolated single grains left over from dating by laserprobe step heating (Huet *et al.* 2015). These authors concluded that the high-Si phengite crystallized during the HP/LT stage, whereas white mica with lower Si-values formed together with chloritized biotite during later retrogression. Two of the Ar–Ar-dated phengite grains had Si-rich cores and Si-poor rims (fig. 3 in Huet *et al.* 2015). Judging from the coincidence of the Ar–Ar plateau and total fusion ages (Huet *et al.* 2015), the volume proportion of the low-Si rims was small and had a negligible influence on the overall age.

For the newly dated samples, we determined the phengite chemistry of separated grains from the same mineral concentrates that were used for preparation of aliquots for Rb–Sr isotope analyses, according to the same screening criteria. In the case of the Fellos samples 5776 and 8104, no significant compositional differences were recognized between individual grain-size fractions, and many of the Si-values cluster around 3.3–3.2 (Fig. 5). On the other hand, EMP *in situ* measurements of randomly selected spots clearly indicate the existence of a bimodal phengite population (Fig. 5a, d). Since the micas of these samples were only enriched by adherence to a piece of paper and not by magnetic properties, a selective pre-concentration during earlier mineral separation steps can be ruled out. In both samples, the mica grains are often very rich in opaque phases. A plausible explanation for the lack of the high-Si micas in the group of separated grains is that such grains were removed during handpicking under the binocular microscope because of abundant inclusions or signs of alteration.

Owing to disturbance of the Rb–Sr isotope system, samples 5776 and 8104 only yielded errorchrons (Fig. 8a), which document a combination of incomplete resetting and partial recrystallization. The larger phengite grain-size fractions do not fit on a common regression line with the smaller grain-size fractions. The apparent lack of a correlation between the Si-values of the various mica sieve fractions and their deviation from a common Rb–Sr regression line suggests that readjustment of the major elements and isotopic characteristics are not correlated or that mixing of the mica populations is not fully reflected by the available EMP data.

The coarser (>355 µm) phengite fractions of samples 5776 (A & B) and 8104 (B & C) lie on a trend indicating a Rb–Sr age of *c.* 117 Ma (Fig. 8a). As these samples were collected close to each other from the same lithologic horizon, it can be reasonably assumed that they had the same or a very similar initial ^{87}Sr/^{86}Sr value. The smaller grain-size fractions alone define trends consistent with various Miocene dates (Fig. 8a). In the case of sample 5776, the apparent age of phengite grains <425 µm (sieve fractions C–L) is *c.* 21 Ma (Fig. 8a; Table 1). A subset of sample 8104 phengite analyses (<355 µm, sieve fractions D–M) yielded an errorchron date of 15 ± 6 Ma (Fig. 8a; Table 1).

Scatter observed for replicate analyses of the same or a similar grain-size range indicate that the original (*in situ*) grain-size distribution has not been completely preserved by sieving. Individual sieve fractions comprise different proportions of whole grains of the given sieve size and fragments of larger grains. However, this mixing effect is only of limited importance because handpicking has apparently removed the older high-Si phengites.

The smaller phengite sieve fractions mainly consist of grains recording younger, deformation-related apparent ages with some fragments of coarser-grained, low-Si phengite that had already undergone partial resetting. As such, different sieve size fractions record different degrees of partial re-equilibration because of mixing during the crushing process, but these fractions are dominated by more strongly overprinted phengite.

We speculate that the Miocene dates are not a fortuitous result but most likely represent different increments of mica recrystallization during post-HP metamorphic deformation. There is a clear trend towards younger apparent ages for the smaller phengite grain-size fractions suggesting deformation-related resetting and synkinematic recrystallization of an older, presumably Cretaceous mica population. The Miocene dates cannot be linked with blueschist-facies metamorphism, but they do correspond very well to apparent ages for greenschist-facies overprinting and related tectonic processes in the nappe stack of the Cycladic Blueschist Unit (e.g. Ring *et al.* 2010; Bröcker *et al.* 2013; Glodny & Ring, 2022 and references therein). The Cretaceous $^{40}Ar–^{39}Ar$ dates from the Fellos area could not be reproduced by Rb–Sr dating, but this is not indicative for contamination by extraneous Ar, but rather results from dating of different mica generations. For $^{40}Ar–^{39}Ar$ laserprobe step heating, Huet *et al.* (2015) used phengite grains of the 0.5–1 mm size fraction. These larger grains are more likely to retain their original Si-values and age than the size fractions used for Rb–Sr dating but are poorly represented in the newly dated samples. We speculate that $^{40}Ar–^{39}Ar$ dating of smaller phengite grain sizes would also provide post-Cretaceous dates and that Rb–Sr dating on larger grain-size fractions than measured here would return Cretaceous ages.

Huet *et al.* (2015) suggested that the different Ar–Ar dates (*c.* 116 and *c.* 106 Ma) correspond to peak metamorphic conditions and a later stage on the retrogression path, respectively, but the presumed link between white mica composition and Ar–Ar dates could not be documented. Although we largely agree with this interpretation, the geological significance of the youngest Ar–Ar date remains ambiguous as the K–Ar system could have been disturbed at various stages during exhumation. We consider a relationship to Miocene deformation as a reasonable possibility.

In the Fellos area, intense localized ductile shear led to partial recrystallization of phengite in garnet-glaucophane schists at ~50–100 m above the original tectonic contact. This process had almost no retrograde effect on associated glaucophane. The Miocene Rb–Sr dates are likely related to the formation of the Fellos shear zone (Xypolias *et al.* 2018), which overprinted and transposed the original nappe contact during exhumation. This is also supported by the fact that blueschist-facies D2 microstructures on both sides of the tectonic contact indicate that the tectonic juxtaposition of the Makrotantalon Unit with the Lower Unit occurred before or during earlier HP/LT metamorphism. The Fellos shear zone is a NE-striking, dextral transpressional zone that developed in the short limb of an inclined antiform and can be mapped along strike over at least 1.5 km with a thickness of ~250 m (Xypolias *et al.* 2018). The Rb–Sr dated samples record strain localization below serpentinites that outline the upper boundary of the shear zone.

Although the picture turned out to be more complicated than expected, the geological relevance of Cretaceous HP/LT metamorphism in the Makrotantalon Unit is also confirmed by Rb–Sr geochronology. The epidote-glaucophane schist 8111, which was collected in a different part of the study area, yielded an apparent age of 121 ± 5 Ma (Fig. 8b). This sample also records disturbance of

the Rb–Sr isotopic system, mainly affecting the <180 μm size fractions, but the Cretaceous age was preserved by the larger phengite grains.

6.b. Eocene HP/LT metamorphism in the Makrotantalon Unit?

The subdivision of the Cycladic nappe stack into distinct subunits is often problematic, and the geology of NW Andros illustrates this situation very well. Gerogiannis *et al.* (2019) concluded that the Makrotantalon Unit is an integral part of the Cycladic Blueschist Unit because their field observations and structural analysis indicated that the sampling location of a blueschist-facies rock with an Eocene age (45.7 ± 3.2 Ma; Bröcker & Franz, 2006) from the Fellos area, originally interpreted as part of the Lower Unit, is instead located in the Makrotantalon Unit. The map of Gerogiannis *et al.* (2019) also indicated a new tectonic assignment for greenschist-facies samples with similar Rb–Sr dates (45 −38 Ma) that were also previously interpreted to belong to the Lower Unit (Huyskens & Bröcker, 2014). Combined with the lack of HP/LT evidence in the Upper Cycladic Unit, the revised structural position of samples with Eocene ages was a key argument for linking the Makrotantalon Unit with the nappe stack of the Cycladic Blueschist Unit, and the interpretation that both share a common post-Cretaceous tectonometamorphic history (Gerogiannis *et al.* 2019). Despite considerable progress in understanding of the contact relationships, the exact position of the tectonic contact at the base of the Makrotantalon Unit remains ambiguous. Trace-element data from ultramafic rocks collected on both sides of the newly defined tectonic contact reveal almost identical geochemical characteristics, possibly indicating the existence of a wider fault zone (Höhn *et al.* 2022). Structural and mineralogical similarities on both sides of the tectonic contact and the lobate pattern for the fault zone, interpreted to result from complex exhumation-related folding (Gerogiannis *et al.* 2019), may have locally obscured identification of the exact position of the tectonic contact and thus the correct structural assignment of samples collected near the inferred nappe boundary. However, the interpretation that the Makrotantalon Unit records Eocene HP/LT metamorphism is supported by Rb–Sr dates (39.9 ± 1.1 Ma and 44.3 ± 1.8 Ma; Fig. 8c, d) for two newly dated epidote-glaucophane schists (samples 10AD37 and 8192B), which were collected at a greater distance from the tectonic contact than the sampling location of the Fellos area (Bröcker & Franz, 2006). Despite the high MSWD values, the most straightforward explanation for the trends shown (Fig. 8c, d) is a basically isochronous relationship, where either full initial isotopic equilibration was not achieved, or a later disturbance occurred without erasing the original age. Both newly dated samples were affected by a greenschist-facies overprint as indicated by the presence of secondary chlorite and albite. There is no obvious link to retrograde deformation and thus the scatter in the isochron diagrams (Fig. 8e, f) is ascribed to disturbance of the Rb–Sr isotope system during fluid-assisted overprinting at lower pressure.

Bröcker *et al.* (2016) reported U–Pb zircon ages of siliciclastic rocks from Andros which indicated maximum depositional ages of ~260 Ma for the Makrotantalon Unit and of 150–125 Ma for the Lower Unit. According to more recent findings, however, the sampling location of the garnet-glaucophane schist 5775, originally interpreted to represent the topmost part of the Lower Unit (Bröcker *et al.* 2016), corresponds instead to the lowermost part of the Makrotantalon Unit (Huet *et al.* 2015; Xypolias *et al.* 2018; Gerogiannis *et al.* 2019). This sample was collected close

to the Rb–Sr dated samples 5776 and 8104 and represents the same rock type that yielded the Cretaceous ^{40}Ar–^{39}Ar dates (Huet *et al.* 2015). The youngest zircon rim age (43.9 ± 4.8 Ma; 2σ) of the detrital population closely corresponds to the Rb–Sr date of the HP/LT schist (45.7 ± 3.2 Ma; Bröcker & Franz, 2006) collected nearby, and clearly documents the influence of Eocene zircon-forming processes on rocks recording Cretaceous blueschist-facies metamorphism. A relationship to the Eocene HP/LT event is a plausible interpretation.

6.c. Is the Makrotantalon Unit an integral part of the Cycladic Blueschist Unit?

Early Cretaceous ages (~116 Ma) of blueschist-facies rocks clearly distinguish the Makrotantalon Unit from other subunits of the Cycladic Blueschist Unit, which lack conclusive evidence for a pre-Eocene metamorphic history. Together with Late Cretaceous dates (~100–90 Ma and ~80–70 Ma) for greenschist-facies rocks from the same tectonic unit, these ages suggest a correlative relationship to the Pelagonian Zone on the Greek mainland (Bröcker & Franz, 2006; Huet *et al.* 2015). The geological relevance of Cretaceous ^{40}Ar–^{39}Ar dates of glaucophanes from south Evia (~120–110 Ma; Maluski *et al.* 1981) has not been corroborated yet, but these apparent ages broadly correspond to the Cretaceous white mica dates of the Makrotantalon Unit (Huet *et al.* 2015; this study), suggesting geological significance and a similar correlative relationship.

Huet *et al.* (2015) assumed that the metamorphic evolution of the Makrotantalon Unit includes a Cretaceous HP/LT event but not an Eocene one, and that both the Makrotantalon Unit and the structurally lower Cycladic Blueschist Unit were affected by the same lower pressure history. Following the hypothesis of tectonic emplacement at ~40 Ma (Huyskens & Bröcker 2014), Huet *et al.* (2015) assumed that the Cycladic Blueschist Unit was affected by blueschist-facies metamorphism when the Pelagonian-derived Makrotantalon Unit was still a part of the upper plate of the subduction system. This led Huet *et al.* (2015) to the conclusion that the tectonic contact at the base of the Makrotantalon Unit was a normal fault and not a thrust (Papanikolaou, 1978b; Huyskens & Bröcker, 2014). However, confirmation of additional Eocene HP/LT metamorphism is at variance to a model that postulates a normal fault at the base of the Makrotantalon Unit.

The existence of Eocene blueschists is a key argument for the interpretation that the Makrotantalon Unit is an integral part of the Cycladic Blueschist Unit (Gerogiannis *et al.* 2019). However, a relationship to the nappe stack of the Cycladic Blueschist Unit cannot unambiguously be deduced from geochronological data alone, because Eocene HP/LT rocks have also been described from the Pelagonian Zone (Schermer *et al.* 1990; Lips *et al.* 1998, 1999).

The NW-trending Pelagonian Zone represents the westernmost part of the Internal Hellenides and includes rock sequences that have undergone Cretaceous to Eocene blueschist- and greenschist-facies metamorphism (e.g. Schermer, 1990; Schermer *et al.* 1990; Lips *et al.* 1998, 1999). The main occurrences of such rocks are the Mt Olympos and Ossa tectonic windows (Fig. 1a) where a weakly metamorphosed sequence of autochthonous platform carbonates and phyllitic rocks is overlain by an allochthonous basement with Hercynian granites and gneisses. In contrast to the HP/LT rocks of the Cyclades (including the Makrotantalon Unit), which have reached *P–T* conditions of the eclogite- to epidote-blueschist-facies (e.g. Huet *et al.* 2015; Laurent *et al.* 2018), lower grade metamorphic conditions were estimated for the
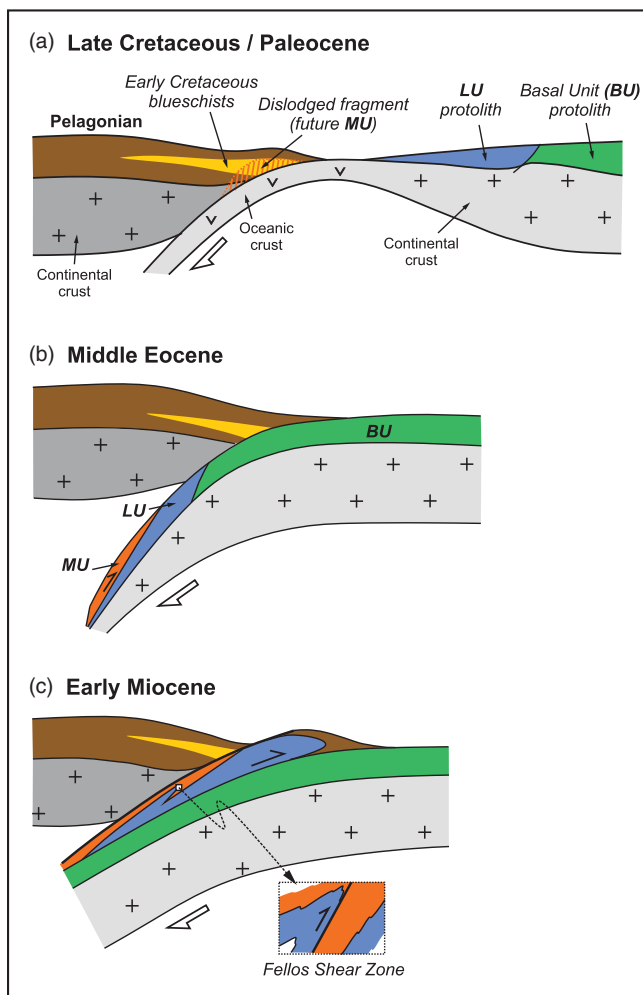
Fig. 9. (Colour online) Proposed tectonic model for the study area from the Late Cretaceous to the Miocene showing the inferred sequence of events that led to incorporation of the Pelagonian Makrotantalon Unit into the nappe stack of the Cycladic Blueschist Unit and the subsequent exhumation (modified after Gerogiannis *et al.* 2019; see text for explanation).

Pelagonian blueschist-greenschist and blueschist-facies rocks (Mt Olympos: <350–500 °C and 0.5–0.8 GPa, Schermer *et al.* 1990; Ossa: 350 °C and 0.8 GPa, Lips *et al.* 1998). Schermer *et al.* (1990) reported multigrain ^{40}Ar–^{39}Ar and Rb–Sr isochron dates indicating four major deformational and metamorphic events at ~293 Ma, ~100 Ma, 61–53 Ma and 40–36 Ma. The oldest ages represent crystallization and cooling of the granitic basement sequence. Apparent ages of ~100 Ma in the autochthonous sequences were interpreted as time constraints of greenschist- to blueschist-facies metamorphism and contemporaneous tectonic stacking of thrust sheets. The age groups at 61–53 Ma and 40–36 Ma were related to blueschist-facies metamorphism and thrusting of blueschists over a carbonate platform, respectively (Schermer *et al.* 1990). Still younger ages between 23 Ma and 16 Ma were linked to uplift and cooling below 150 °C. On the basis of single-grain ^{40}Ar–^{39}Ar laserprobe dating, Lips *et al.* (1998, 1999) concluded that HP/LT metamorphism in the Ossa tectonic window and the southern Pelion Massif began at ~100–85 Ma and ceased at ~54 Ma, followed by greenschist-facies metamorphism that ended in the Ossa–Olympos region by 40–36 Ma but continued in the Pelion Massif until 15 Ma.

Similarities in the post-Cretaceous geochronological record of the Pelagonian Zone and the Cycladic Blueschist Unit alone do not provide an obvious argument for an unambiguous assignment of the Makrotantalon Unit to the nappe stack of the Cycladic Blueschist Unit. However, microstructural observations further support this interpretation. Gerogiannis *et al.* (2019) related the main ductile deformation phase affecting both tectonic units exposed in NW Andros to tectonic stacking. A well-preserved penetrative to mylonitic blueschist-facies foliation on both sides of the tectonic contact was linked to the Eocene HP/LT event that is recorded on a regional scale in the Cyclades. An earlier deformation phase at blueschist-facies conditions is only preserved within the Makrotantalon Unit and is possibly associated with the Cretaceous HP/LT event (Gerogiannis *et al.* 2019). Combined, these observations further substantiate the interpretation that the Miocene dates of the Fellos samples are related to tectonic transposition of the contact between the two nappes during exhumation. Despite its Pelagonian origin (Huet *et al.* 2015), the Makrotantalon Unit is now an integral part of the Cycladic Blueschist Unit with a common metamorphic history from Eocene time onwards (Gerogiannis *et al.* 2019). The inferred sequence of events that led to the incorporation of the Pelagonian Makrotantalon Unit into the nappe stack of the Cycladic Blueschist Unit is schematically shown in Figure 9. This model follows Gerogiannis *et al.* (2019), who suggested tectonic juxtaposition of these units at deep subduction levels during Eocene time or somewhat earlier, resulting in a common metamorphic history since that time.

7. Summary and conclusion

Using Rb–Sr geochronology, we dated blueschist-facies rocks from the Makrotantalon Unit on Andros, Greece. We assume that all samples were originally fully equilibrated on the whole-rock scale under HP/LT conditions at different times. The poor linear fit in the multi-point isochron diagrams and related high MSWD values indicate scatter in excess of analytical uncertainty, resulting from disturbance of the Rb–Sr isotope system during post-HP/LT metamorphic processes. This study is not providing high-precision geochronology, but rather shows that a disturbed dataset can still make sense in the regional chronological framework. The new apparent ages are consistent with existing Ar–Ar and Rb–Sr data of similar rocks from the study area and are considered to place geologically meaningful constraints on the time of two distinct blueschist-facies events that occurred *c.* 60–70 Ma apart.

The results of this study clearly show that the Makrotantalon Unit was affected by both Cretaceous and Eocene HP/LT episodes, and they substantiate interpretations suggesting that the Makrotantalon Unit represents a tectonic slice with Pelagonian affinity in the nappe stack of the Cycladic Blueschist Unit (Huet *et al.* 2015; Gerogiannis *et al.* 2019). The studied samples are affected by incomplete re-equilibration of the Rb–Sr isotope system and document a combination of inheritance from the HP/LT stage and partial recrystallization during lower pressure overprinting and deformation. The smaller grain-size fractions yielded Miocene Rb–Sr dates that are related to synkinematic recrystallization of micas during the formation of exhumation-related shear zones, which have transposed the original thrust contact. These dates are consistent with apparent ages of greenschist-facies rocks from the Lower Unit on Andros and elsewhere in the Cycladic Blueschist Unit. Epidote-glaucophane schists collected at a greater distance from the tectonic contact in other parts of the

Makrotantalon Unit are also characterized by disturbed isochrons, but a relationship to tectonic stacking or later fault reactivation is not evident from observations and data. As glaucophane is partially replaced by retrograde phases, the scatter in the isochron plots can broadly be associated with greenschist-facies overprinting. The Rb–Sr dates of such samples (*c.* 121 Ma, *c.* 40 Ma and *c.* 44 Ma) further substantiate the significance of both Cretaceous and Eocene blueschist-facies events in the Makrotantalon Unit.

References

Altherr R, Kreuzer H, Wendt I, Lenz H, Wagner GA, Keller J, Harre W and Höhndorf A (1982) A Late Oligocene/Early Miocene high temperature belt in the Attic-Cycladic Crystalline Complex (SE Pelagonian, Greece). *Geologisches Jahrbuch* E **23**, 97–164.

Altherr R, Schliestedt M, Okrusch M, Seidel E, Kreuzer H, Harre W, Lenz H, Wendt I and Wagner GA (1979) Geochronology of high-pressure rocks on Sifnos (Cyclades, Greece). *Contributions to Mineralogy and Petrology* **70**, 245–55.

Aravadinou E, Xypolias P, Chatzaras V, Iliopoulos I and Gerogiannis N (2016) Ductile nappe stacking and refolding in the Cycladic Blueschist Unit: insights from Sifnos Island (south Aegean Sea). *International Journal of Earth Sciences* **105**, 2075–96.

Avigad D and Garfunkel Z (1991) Uplift and exhumation of high-pressure metamorphic terrains; the example of the Cycladic blueschist belt (Aegean Sea). *Tectonophysics* **188**, 357–72.

Avigad D, Garfunkel Z, Jolivet L and Azañon JM (1997) Back arc extension and denudation of Mediterranean eclogites. *Tectonics* **16**, 924–41.

Bröcker M, Baldwin S and Arkudas R (2013) The geologic significance of ^{40}Ar/^{39}Ar and Rb–Sr white mica ages from Syros and Sifnos, Greece: a record of continuous (re)crystallization during exhumation? *Journal of Metamorphic Geology* **31**, 629–46. doi: 10.1111/jmg.12037.

Bröcker M and Enders M (1999) U–Pb zircon geochronology of unusual eclogite-facies rocks from Syros and Tinos (Cyclades, Greece). *Geological Magazine* **136**, 111–18.

Bröcker M and Franz L (2006) Dating metamorphism and tectonic juxtaposition on Andros Island (Cyclades, Greece): results of a Rb–Sr study. *Geological Magazine* **143**, 609–20.

Bröcker M, Huyskens M and Berndt J (2016) U–Pb dating of detrital zircons from Andros, Greece: constraints for the time of sediment accumulation in the northern part of the Cycladic blueschist belt. *Geological Journal* **51**, 354–67.

Bröcker M and Keasling A (2006) Ionprobe U–Pb zircon ages from the high-pressure/low-temperature mélange of Syros, Greece: age diversity and the importance of pre-Eocene subduction. *Journal of Metamorphic Geology* **24**, 615–31.

Bröcker M, Kreuzer H, Matthews A and Okrusch M (1993) ^{40}Ar/^{39}Ar and oxygen isotope studies of polymetamorphism from Tinos Island, Cycladic blueschist belt. *Journal of Metamorphic Geology* **11**, 223–40.

Bröcker M and Pidgeon RT (2007) Protolith ages of meta-igneous and meta-tuffaceous rocks from the Cycladic blueschist unit, Greece: results of a reconnaissance U–Pb zircon study. *Journal of Geology* **115**, 83–98.

Bulle F, Bröcker M, Gärtner C and Keasling A (2010) Geochemistry and geochronology of HP mélanges from Tinos and Andros, Cycladic blueschist belt, Greece. *Lithos* **117**, 61–81.

Cliff RA, Bond CE, Butler RWH and Dixon JE (2017) Geochronological challenges posed by continuously developing tectonometamorphic systems,

insights from Rb–Sr mica ages from the Cycladic Blueschist Belt, Syros (Greece). *Journal of Metamorphic Geology* **35**, 197–211.

Doutsos T, Pe-Piper G, Boronkay K and Koukouvelas I (1993) Kinematics of the central Hellenides. *Tectonics* **12**, 936–53.

Dragovic B, Baxter EF and Caddick MJ (2015) Pulsed dehydration and garnet growth during subduction revealed by zoned garnet geochronology and thermodynamic modeling, Sifnos, Greece. *Earth and Planetary Science Letters* **413**, 111–22.

Dürr S (1986) Das Attisch–Kykladische Kristallin. In *Geologie von Griechenland* (ed. V Jacobshagen), pp. 116–48. Berlin: Bornträger.

Dürr S, Altherr R, Keller J, Okrusch M and Seidel E (1978) The Median Aegean Crystalline Belt: stratigraphy, structure, metamorphism, magmatism. In *Alps, Appeninnes, Hellenides* (eds H Closs, DH Roeder and K Schmidt), pp. 455–77. Stuttgart: Schweizerbart.

Forster MA and Lister GS (2005) Several distinct tectono-metamorphic slices in the Cycladic eclogite–blueschist belt, Greece. *Contributions to Mineralogy and Petrology* **150**, 523–45.

Fu B, Valley JW, Kita NT, Spicuzza MJ, Paton C, Tsujimori T, Bröcker M and Harlow GE (2010) Multiple origins of zircons in jadeitite. *Contributions to Mineralogy and Petrology* **159**, 769–80. doi: 10.1007/s00410-009-0453-y.

Gerogiannis N and Xypolias P (2017) Retroward extrusion of high-pressure rocks: an example from the Hellenides (Pelion Blueschist Nappe, NW Aegean). *Terra Nova* **29**, 372–81.

Gerogiannis N, Xypolias P, Chatzaras V, Aravadinou E and Papapavlou K. (2019) Deformation within the Cycladic subduction-exhumation channel: new insights from the enigmatic Makrotantalo nappe (Andros, Aegean). *International Journal of Earth Science* **108**, 817–43.

Glodny J and Ring U (2022) The Cycladic Blueschist Unit of the Hellenic subduction orogen: protracted high-pressure metamorphism, decompression and reimbrication of a diachronous nappe stack. *Earth-Science Reviews* **224**, 103883. doi: 10.1016/j.earscirev.2021.103883.

Halama R, Glodny J, Konrad-Schmolke M and Sudo M (2018) Rb–Sr and in situ ^{40}Ar/^{39}Ar dating of exhumation-related shearing and fluid-induced recrystallization in the Sesia zone (Western Alps, Italy). *Geosphere* **14**, 1425–50.

Harrison TM, Celerier J, Aikman AB, Hermann J and Heizler MT (2009) Diffusion of ^{40}Ar in muscovite. *Geochimica et Cosmochimica Acta* **73**, 1039–51.

Höhn M, Bröcker M and Berndt J (2022) The Jurassic meta-ophiolitic rocks of Cape Steno, Andros, Greece: a high-pressure/low-temperature mélange with Pelagonian affinity in the Cycladic Blueschist Unit? *International Journal of Earth Sciences* **111**, 949–68.

Huet B, Labrousse L, Monié P, Malvoisin B and Jolivet L (2015) Coupled phengite ^{40}Ar–^{39}Ar geochronology and thermobarometry: *P-T-t* evolution of Andros Island (Cyclades, Greece). *Geological Magazine* **152**, 711–27.

Huyskens M and Bröcker M (2014) The status of the Makrotantalon Unit (Andros, Greece) within the structural framework of the Attic-Cycladic Crystalline Belt. *Geological Magazine* **151**, 430–46.

Kalsbeek F and Hansen M (1989) Statistical analysis of Rb–Sr isotope data by the "bootstrap" method. *Chemical Geology, Isotope Geoscience Section* **73**, 289–97.

Katzir Y, Avigad D, Matthews A, Garfunkel Z and Evans BW (2000) Origin, HP/LT metamorphism and cooling of ophiolitic melanges in southern Evia (NW Cyclades), Greece. *Journal of Metamorphic Geology* **18**, 699–718.

Kelley S (2002) Excess argon in K–Ar and Ar–Ar geochronology. *Chemical Geology* **188**, 1–22.

Kurzawa T, Bröcker M, Fotoohi Rad GR, Berndt J and Lisker F (2017) Cretaceous high-pressure metamorphism and low-pressure overprint in the Sistan Suture Zone, eastern Iran: additional temperature estimates for eclogites, geological significance of U–Pb zircon ages and Rb–Sr constraints on the timing of exhumation. *Journal of Asian Earth Sciences* **147**, 332–44.

Lagos M, Scherer EE, Tomaschek F, Münker C, Keiter M, Berndt J and Ballhaus C (2007) High precision Lu/Hf geochronology of Eocene eclogite facies rocks from Syros, Cyclades, Greece. *Chemical Geology* **243**, 16–35.

Lamont TN, Roberts NMW, Searle MP, Gopon P, Waters DJ and Millar I (2020a) The age, origin, and emplacement of the Tsiknias Ophiolite, Tinos, Greece. *Tectonics* **39**, e2019TC005677. doi: 10.1029/2019TC005677.

Lamont TN, Searle MP, Gopon P, Roberts NMW, Wade J, Palin RM, Waters DJ (2020b) The Cycladic Blueschist Unit on Tinos, Greece: cold NE subduction and SW directed extrusion of the Cycladic continental margin under the Tsiknias Ophiolite. *Tectonics* **39**, e2019TC005890. doi: 10.1029/2019TC005890.

Laurent V, Huet B, Labrousse L, Jolivet L, Monie P and Augier R (2017) Extraneous argon in high-pressure metamorphic rocks: distribution, origin and transport in the Cycladic Blueschist Unit (Greece). *Lithos* **272**, 315–35.

Laurent V, Lanari P, Naïr I, Augier R, Lahfid A and Jolivet L (2018) Exhumation of eclogite and blueschist (Cyclades, Greece): pressure–temperature evolution determined by thermobarometry and garnet equilibrium modelling. *Journal of Metamorphic Geology* **36**, 769–98.

Leake BF, Woolley AR, Arps CES, Birch WD, Gilbert MC, Grice JD, Hawthorne FC, Kato A, Kisch HJ, Krivovichev VG, Linthout K, Laird J, Mandarino JA, Maresch WV, Nickel EH, Rock NMS, Schumacher JC, Smith DC, Stephenson NCN, Ungaretti L, Whittaker EJW and Youzhi G (1997) Nomenclature of amphiboles: report of the subcommittee on amphiboles of the International Mineralogical Association, commission on new minerals and mineral names. *American Mineralogist* **82**, 1019–37.

Lips ALW, White SH and Wijbrans JR (1998) ^{40}Ar/^{39}Ar laserprobe direct dating of discrete deformational events: a continuous record of early Alpine tectonics in the Pelagonian Zone, NW Aegean area, Greece. *Tectonophysics* **298**, 133–53.

Lips ALW, Wijbrans JR and White SH (1999) New insights from ^{40}Ar/^{39}Ar laserprobe dating of white mica fabrics from the Pelion Massif, Pelagonian Zone, Internal Hellenides, Greece: implications for the timing of metamorphic episodes and tectonic events in the Aegean region. In *The Mediterranean Basins: Tertiary Extension within the Alpine Orogen* (eds B Durand, L Jolivet, F Horvàth and M Séranne), pp. 456–74. Geological Society of London, Special Publication no. 156.

Locock AJ (2014) An Excel spreadsheet to classify chemical analyses of amphiboles following the IMA 2012 recommendations. *Computers & Geosciences* **62**, 1–11.

Ludwig KR (2012) User's Manual for ISOPLOT version 3.75–4.15: Geochronological Toolkit for Microsoft Excel. Berkeley Geochronology Center, Special Publication no. 5.

Maluski H, Vergely P, Bavay D, Bavay P and Katsikatsos G (1981) ^{39}Ar/^{40}Ar dating of glaucophanes and phengites in southern Euboa (Greece) geodynamic implications. *Bulletin de la Société géologique de France* **5**, 469–76.

Martha SO, Dörr W, Gerdes A, Petschick R, Schastok J, Xypolias P and Zulauf G (2016) New structural and U–Pb zircon data from Anafi crystalline basement (Cyclades, Greece): constraints on the evolution of a Late Cretaceous magmatic arc in the Internal Hellenides. *International Journal of Earth Sciences* **105**, 2031–60.

Massonne HJ and Schreyer W (1987) Phengite geobarometry based on the limiting assemblage with K-feldspar, phlogopite, and quartz. *Contributions to Mineralogy and Petrology* **96**, 212–24.

Matthews A and Schliestedt M (1984) Evolution of the blueschist and greenschist-facies rocks of Sifnos, Cyclades, Greece: a stable isotope study of subduction related metamorphism. *Contributions to Mineralogy and Petrology* **88**, 150–63.

Mehl C, Jolivet L, Lacombe O, Labrousse L and Rimmele G (2007) Structural evolution of Andros (Cyclades, Greece): a key to the behaviour of a (flat) detachment within an extending continental crust. In *The Geodynamics of the Aegean and Anatolia* (eds T Taymaz, Y Yilmaz and Y Dilek), pp. 41–73. Geological Society of London, Special Publication no. 291.

Mukhin P (1996) The metamorphosed olistostromes and turbidites of Andros Island, Greece, and their tectonic significance. *Geological Magazine* **133**, 697–711.

Nebel O, Mezger K, Scherer E and Münker C (2005) High precision determinations of ^{87}Rb/^{85}Rb in geologic materials by MC-ICP-MS. *International Journal of Mass Spectrometry* **246**, 10–18.

Okrusch M and Bröcker M (1990) Eclogite facies rocks in the Cycladic blueschist belt, Greece: a review. *European Journal of Mineralogy* **2**, 451–78.

Papanikolaou D (1978a) Geologic Map of Greece. Andros Island, 1:50.000. Athens: Institute of Geological and Mining Research (IGME).

Papanikolaou D (1978b) Contribution to the geology of the Aegean Sea; the island of Andros. *Annales Géologiques des Pays Helléniques* **29**, 477–553.

Papanikolaou D (1987) Tectonic evolution of the Cycladic blueschist belt (Aegean Sea, Greece). In *Chemical Transport in Metasomatic Processes* (ed. HC Helgeson), pp. 429–50. Dordrecht: Reidel.

Papanikolaou D (2013) Tectonostratigraphic models of the Alpine terranes and subduction history of the Hellenides. *Tectonophysics* **595–596**, 1–24.

Parra T, Vidal O and Jolivet L (2002) Relation between the intensity of deformation and retrogression in blueschist metapelites of Tinos Island (Greece) evidenced by chlorite-mica local equilibria. *Lithos* **63**, 41–66.

Patzak M, Okrusch M and Kreuzer H (1994) The Akrotiri unit on the island of Tinos, Cyclades, Greece: witness to a lost terrane of Late Cretaceous age. *Neues Jahrbuch für Geologie und Paläontologie Abhandlungen* **194**, 211–52.

Peillod A, Ring U, Glodny J and Skelton A (2017) An Eocene/Oligocene blueschist/greenschist-facies *P-T* loop from the Cycladic Blueschist Unit on Naxos Island, Greece: deformation-related reequilibration vs thermal relaxation. *Journal of Metamorphic Geology* **35**, 805–30.

Philippon M, Brun J-P and Gueydan F (2012) Deciphering subduction from exhumation in the segmented Cycladic Blueschist Unit (Central Aegean, Greece). *Tectonophysics* **524–525**, 116–34.

Purdy JW and Jäger E (1976) K–Ar ages on rock-forming minerals from the Central Alps. *Memoirs of the Institute of Geology and Mineralogy, University of Padova* **30**, 3–31.

Putlitz B, Cosca MA and Schumacher JC (2005) Prograde mica ^{40}Ar/^{39}Ar growth ages recorded in high pressure rocks (Syros, Cyclades, Greece). *Chemical Geology* **214**, 79–98.

Reinecke T (1986) Phase relationships of sursassite and other Mn-silicates in highly oxidized, high-pressure metamorphic rocks from Evia and Andros Islands, Greece. *Contributions to Mineralogy and Petrology* **94**, 110–26.

Reinecke T, Okrusch M and Richter P (1985) Geochemistry of ferromanganoan metasediments from the island of Andros, Cycladic Blueschist Belt, Greece. *Chemical Geology* **53**, 249–78.

Ring U, Glodny J, Will J and Thomson SN (2010) The Hellenic subduction system: high-pressure metamorphism, exhumation, normal faulting, and large-scale extension. *Annual Review of Earth and Planetary Sciences* **38**, 45–76

Scharf A, Handy MR, Schmid SM, Favaro S, Sudo M, Schuster R and Hammerschmidt K (2016) Grain-size effects on the closure temperature of white mica in a crustal-scale extensional shear zone — implications of in-situ ^{40}Ar/^{39}Ar laser-ablation of white mica for dating shearing and cooling (Tauern Window, Eastern Alps). *Tectonophysics* **674**, 210–26.

Schermer ER (1990) Mechanisms of blueschist creation and preservation in an A-type subduction zone, Mount-Olympos Region, Greece. *Geology* **18**, 1130–3.

Schermer ER, Lux DR and Burchfiel BC (1990), Temperature-time history of subducted continental-crust, Mount Olympos Region, Greece. *Tectonics* **9**, 1165–95. doi: 10.1029/TC009i005p01165.

Shaked Y, Avigad D and Garfunkel Z (2000) Alpine high-pressure metamorphism at the Almyropotamos window (southern Evia, Greece). *Geological Magazine* **137**, 367–80.

Stracke A, Scherer EE and Reynolds BC (2014) Application of isotope dilution in geochemistry. In *Treatise on Geochemistry (Second Edition), Volume 15* (eds HD Holland and KK Turekian), pp. 71–86. Oxford: Elsevier.

Tomaschek F, Kennedy A, Villa IM, Lagos M and Ballhaus C (2003) Zircons from Syros, Cyclades, Greece—recrystallization and mobilization of zircon during high-pressure metamorphism. *Journal of Petrology* **44**, 1977–2002.

Villa I, De Bièvre P, Holden N and Renne P (2015) IUPAC-IUGS recommendation on the half life of ^{87}Rb. *Geochimica et Cosmochimica Acta* **164**, 382–5.

von Blanckenburg F, Villa IM, Baur H, Morteani G and Steiger RH (1989) Time calibration of a PT-path from the Western Tauern Window, Eastern Alps: the problem of closure temperatures. *Contributions to Mineralogy and Petrology* **101**, 1–11.

Wendt I and Carl C (1991) The statistical distribution of the mean squared weighted deviation. *Chemical Geology* **86**, 275–85.

Wijbrans JR, Schliestedt M and York D (1990) Single grain argon laser probe dating of phengites from the blueschist to greenschist transition on Sifnos (Cyclades, Greece). *Contributions to Mineralogy and Petrology* **104**, 582–93.

Xypolias P, Gerogiannis N, Chatzaras V, Papapavlou K, Kruckenberg SC, Aravadinou E and Michels Z (2018) Using incremental elongation and shearing to unravel the deformation path in a complex transpressional zone. *Journal of Structural Geology* **115**, 64–81.

Xypolias P, Iliopoulos I, Chatzaras V and Kokkalas S (2012) Subduction- and exhumation-related structures in the Cycladic Blueschists: insights from south Evia Island (Aegean region, Greece). *Tectonics* **31**, TC2001. doi: 10.1029/2011TC002946.

Xypolias P, Kokkalas S and Skourlis K (2003) Upward extrusion and subsequent transpression as a possible mechanism for the exhumation of HP/LT rocks in Evia Island (Aegean Sea, Greece). *Journal of Geodynamics* **35**, 303–32.